# Intercellular communication between glioma and innate immune cells

Abels, E.R.

# Chapter 3

## Glioblastoma-associated microglia reprogramming is mediated by functional transfer of extracellular miR-21

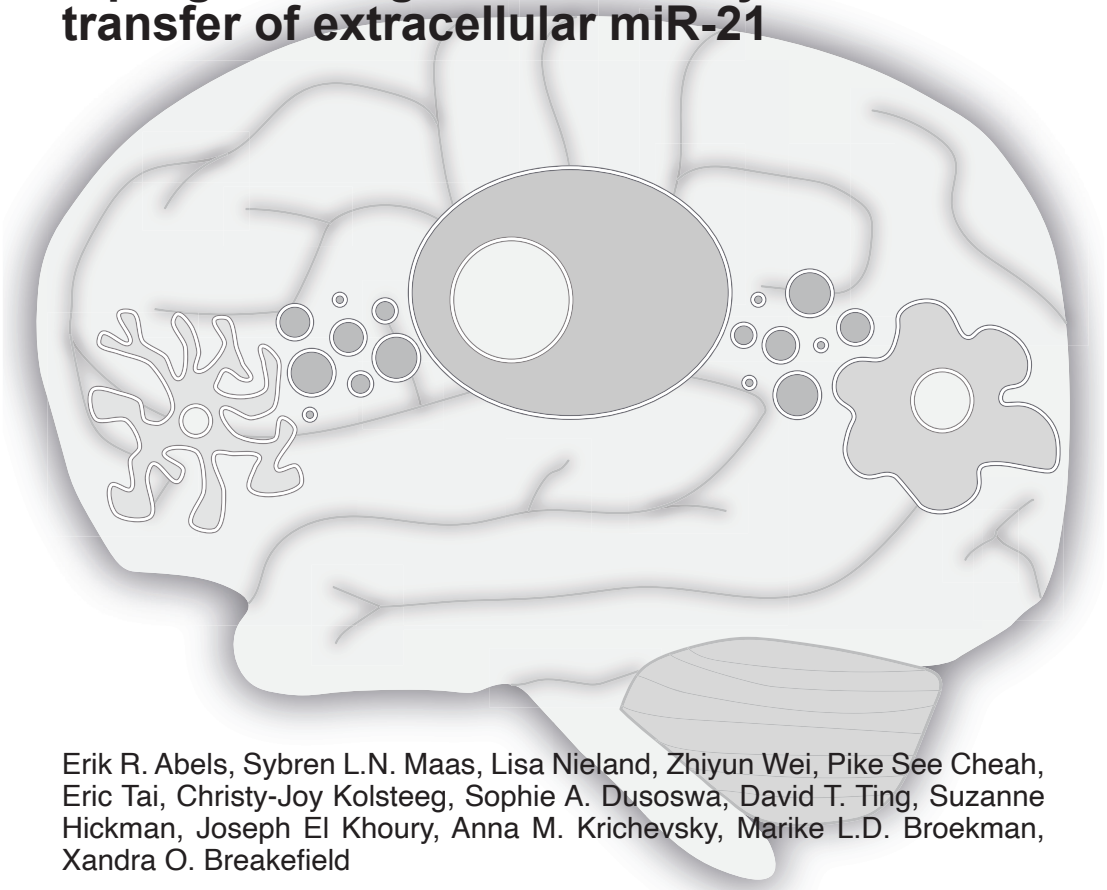

Erik R. Abels, Sybren L.N. Maas, Lisa Nieland, Zhiyun Wei, Pike See Cheah, Eric Tai, Christy-Joy Kolsteeg, Sophie A. Dusoswa, David T. Ting, Suzanne Hickman, Joseph El Khoury, Anna M. Krichevsky, Marike L.D. Broekman, Xandra O. Breakefield

*Cell Reports. 2019*

## Abstract

Gliomas are primary, diffusely infiltrating brain tumors. Microglia are innate immune cells in the central nervous system and make up a substantial portion of the tumor mass. Glioma cells shape their microenvironment communicating with and reprogramming surrounding cells resulting in enhanced angiogenesis, immune suppression and remodeling of the extracellular matrix. Glioma cells communicate with microglia, in part by releasing extracellular vesicles (EVs). Mouse glioma cells, stably expressing a palmitoylated green fluorescent protein (GFP) to label EVs were implanted intracranially into syngeneic miR-21-null mice. Here, we demonstrate functional delivery of miR-21, regulating specific downstream mRNA targets in microglia after uptake of tumor-derived EVs. These finding attest to EV dependent microRNA delivery as studied in an *in vivo* based model and provide insight into the reprograming of microglial cells by tumor cells to create a favorable microenvironment for cancer progression.

## Introduction

Gliomas, including glioblastomas (GBs) are the most common and lethal primary adult brain tumors(Ostrom et al., 2013; Ostrom et al., 2018; Weller et al., 2015). They are characterized and defined by their highly aggressive nature involving rapid tumor growth, diffuse invasiveness and resistance to therapy(Stupp et al., 2009). GBs are made up of a heterogeneous population of tumor cells and various types of stromal cells, which all contribute to tumor progression and resistance to treatment(Broekman et al., 2018; Hambardzumyan et al., 2016; Quail and Joyce, 2017). GB cells exert effects on endogenous central nervous system (CNS) cell types, such as microglia, astrocytes, oligodendrocytes, endothelial cells and neurons as well as infiltrating monocytes/macrophages (MO/Mφ)(Broekman et al., 2018; Quail and Joyce, 2017). Amongst these different cell types, microglia and MO/Mφ are the most prevalent cell types within the tumor(Morantz et al., 1979a, b). Microglia are the resident innate immune cells in the brain(Li and Barres, 2018), whereas MO residing in a tumor have infiltrated from the blood circulation and can subsequently differentiate to Mφ(Bowman et al., 2016). In response to tumor stimuli, these non-tumorigenic cells produce chemokines and cytokines, including growth and angiogenic factors, immunosuppressive molecules and extracellular matrix modifying enzymes, which make the environs favorable to tumor progression(Hambardzumyan et al., 2016; Li and Graeber, 2012).

In addition to soluble factors, GB cells communicate with surrounding cells by release of membrane-bound extracellular vesicles (EVs) containing proteins, lipids and RNA(Maas et al., 2017). Different RNA species are found in their EVs,

including microRNA (miRNA), small nucleolar RNA, Y RNA, mitochondrial RNA, and vault RNA, as well as long non-coding RNA and mRNA(Nolte-'t Hoen et al., 2012; Wei et al., 2017b). EVs are known to carry specific, RNA cargo from donor cells to recipient cells(Skog et al., 2008; Valadi et al., 2007). Since the lipid bilayer of the EVs protects the cargo from degradation, EV contents can be delivered to closely surrounding cells as well as distant recipient cells. Increasing evidence suggests that content can be loaded selectively into EVs, e.g. RNA(Mateescu et al., 2017), and - once transferred - affect the phenotype of recipient cells as studied *in vitro* (de Vrij et al., 2015; Skog et al., 2008; Tkach and Théry, 2016; Valadi et al., 2007; van der Vos et al., 2016).

miRNAs are small RNAs, involved in the target cleavage, translational repression and deadenylation of mRNA(Winter et al., 2009). Among them, miRNA-21 (miR-21) is the most studied in the context of cancer generally, and in glioma specifically. The promoter and mature miRNA sequence for miR-21 is highly conserved across a number of vertebrate species(Krichevsky and Gabriely, 2009), with the transcription of miR-21 regulated through an independent promoter site located in the intron region of a protein-coding gene(Fujita et al., 2008). miR-21 has been shown to play a role in embryogenesis, self-renewal and development in normal cell physiology, but its expression is dysregulated in the context of oncogenic processes(Kumarswamy et al., 2011; Põlajeva et al., 2012). Furthermore, miR-21 expression is associated with cell differentiation, and depending on the model system is shown to induce osteogenic differentiation and inhibit neural stem cell differentiation(Gao et al., 2016; Wei et al., 2017a). In GB it has been shown that miR-21 acts as an important oncogene(Chan et al., 2005; Krichevsky and Gabriely, 2009) as high levels of miR-21 in GB lead to the downregulation of the tumor suppressor gene IGFBP3(Yang et al., 2014) and are associated with activation of metalloproteinases(Gabriely et al., 2008). The expression level of miR-21 is inversely correlated with the survival rate of GB patients(Yang et al., 2014). miR-21 has been identified as a cerebrospinal fluid (CSF) biomarker for monitoring glioma growth and therapy response(Teplyuk et al., 2012). In addition, studies evaluating GB-derived EVs in CSF indicated that elevated miR-21 levels are associated with worse prognosis(Akers et al., 2013; Shi et al., 2015). Interference with miR-21 reduces the malignant potential as downregulation of miR-21 have been shown to inhibit cell proliferation and invasion *in vitro* and tumor progression *in vivo*(Belter et al., 2016; Corsten et al., 2007; Gabriely et al., 2008; Põlajeva et al., 2012).

In this study we investigated the transfer of miRNA by glioma EVs between tumor and stromal cells using miR-21 as the model miRNA. Using a mouse glioma cell line, GL261, stably expressing a palmitoylated fluorescent protein, we monitored the uptake of EVs by microglia and MO/Mφ in the brain(Lai et al., 2015; van der Vos et al., 2016). To avoid interference by endogenous recipient cell miR-21, GL261

cells were implanted in the brains of mice lacking expression of miR-21(Ma et al., 2011). Using this reporter, we were able to study the uptake of naturally shed EV in an *in vivo* setting. This approach avoids many of the technical issues hampering EV research, such as mechanical manipulation, subselecting for specific EV populations during isolation and the injection or incubation with an arbitrary number of EVs are circumvented(Abels et al., 2019; Théry et al., 2018).
Here we demonstrate functional delivery of miR-21 from glioma cells to the surrounding innate immune cells subsequently leading to downregulation of specific miR-21 mRNA targets. Additionally, injection experiments using isolated glioma-derived EVs confirm that the observed effects can be mediated by EVs, although we do not exclude additional involvement of other miR-21 carriers, such as large EV or non-floating non-EV components. Taken together this proves functional EV-mediated miRNA transfer *in vivo* using spontaneously released EVs resulting in reprogramming of microglia.

## Results

### *GL261-derived EVs contain high levels of miR-21*

To study the functional extracellular transfer of miRNAs from tumor to surrounding cells *in vivo,* we use syngeneic mouse glioma cells, GL261.palmGFP.H2B.mRFP (GL261.pGHR) (**Fig. 1A**). GL261 cells expressing a palmitoylated form of green fluorescent protein (GFP) facilitates tracking of the uptake of tumor-derived membrane fragments, including EVs, into stromal cells in the tumor microenvironment(Lai et al., 2015; van der Vos et al., 2016). In addition, the nuclear localized RFP fused to the H2B histone helps to discriminate EV uptake from phagocytosis of whole cells(Welm et al., 2008). Using differential ultracentrifugation (**Fig. 1B**), larger vesicles and cell fragments pelleted at 2000xg, EVs, including exosomes and microvesicles isolated from GL261 cell conditioned medium by centrifugation at 100,000xg. Heterogeneity of these different fractions was confirmed by probing for different vesicular protein markers that are present in all types of EVs and larger vesicle fractions (Flotilin-1)(Kowal et al., 2016), those typically associated with exosomes and absent in 2000xg (ALIX and TSG101), and GAPDH found to be enriched in the 2000xg and cellular fraction(McNamara et al., 2018). Importantly, GFP protein was detected in both cellular and extracellular fractions confirming that this marker can be used to track the fate of all different subtypes of EVs (**Fig. 1C**). Nanoparticle Tracking Analysis (NTA) of the EVs isolated by 100,000xg ultracentrifugation, revealed a broad size distribution of EVs ranging from 100 nm to 500 nm further confirming their heterogeneity (**Supplementary Fig. S1A**). Importantly, miR-21 was present in GL261 cells, 2000xg fraction and

GL261-derived EVs with significantly higher levels of miR-21 in the EVs compared to cellular levels (**Fig. 1D-E**). The level of miR-21 in cells, the 2000xg fraction and EVs was higher than the level of to the miR-10b, a miRNA uniquely expressed in glioma(El Fatimy et al., 2017), as compared to normal brain (**Supplementary Fig. S1B-C**)

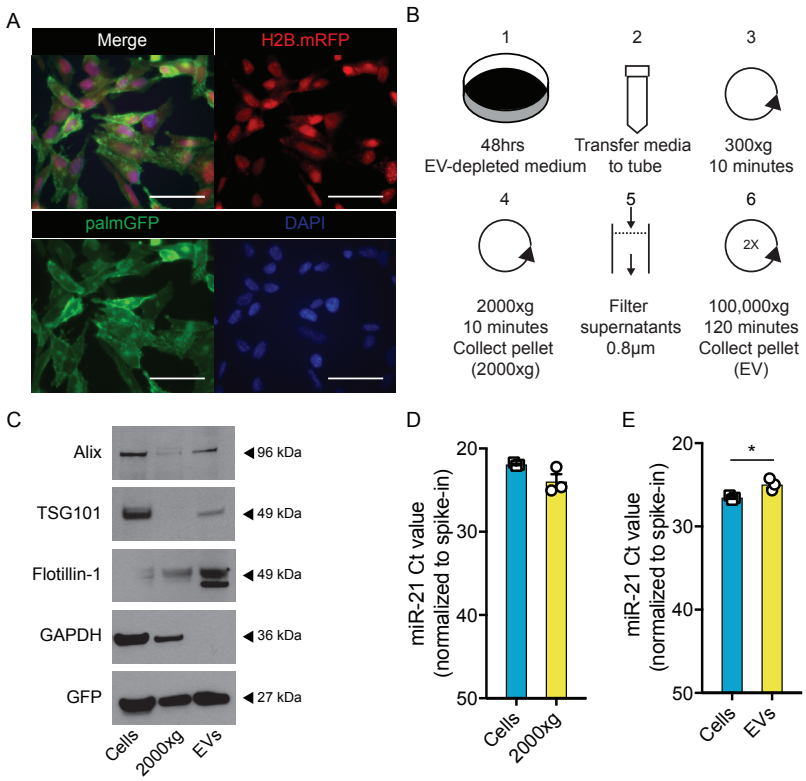


.

**Figure 1. miR-21 is abundantly present in GL261 tumor cells and isolated EV.** (**A**) GL261 cells were transduced to stably express palmitoylated GFP (palmGFP; lower left panel) as membrane marker and the H2B.mRFP (upper right panel) as nuclear marker that colocalized with DAPI (lower right panel). Scale bar 50 µm. (**B**) Schematic overview of EV isolation using differential centrifugation. Pellets acquired after first round of ultracentrifugation were concentrated by second round of ultracentrifugation to obtain purer population of EVs. (**C**) Western blot demonstrates vesicle markers (ALIX and Flottilin-1) excluding TSG101, enriched in EV lysates. GFP was detected in all lysates (equal protein amount loaded). (**D**) Expression level of miR-21 analyzed using RT-qPCR, as plotted in Ct value normalized to spike-in (UniSp6), shows similar levels of miR-21 in cells and 2000xg fraction (**E**) Expression level of miR-21 analyzed using RT-qPCR, as plotted in Ct value normalized to spike-in (UniSp6), shows higher levels of miR-21 in EVs compared to cells. Data represents 3 independent experiments and is presented as the mean with SEM (error bars). $P<0.05$. Unpaired T-test.

To further confirm the presence of miR-21 in EVs, we separated the different sized vesicles collected at 100,000xg and performed an iodixanol gradient. The EVs were bottom loaded and the gradient was performed over 16 hours at 156,000xg (**Supplementary Fig. S2A**). In total, 12 fractions were collected and analyzed for GFP protein levels, as well as miR-21 levels. Overall, miR-21 was found to co-localize with GFP, but miR-21 was also present in the high-density fractions possibly associated with high-density lipoproteins (**Supplementary Fig. S2B-C**) (Vickers et al., 2011). Taken together, the heterogeneous population of EVs shed by tumor cells is labeled with membrane-bound GFP and contains high levels of miR-21.

## *Tumor-derived EVs effectively deliver miR-21 to microglia*

Next, GL261.pGHR cells or carrier fluids were injected in adult miR-21-null mouse brains. By using miR-21-null mice we were able to differentiate between endogenous upregulation of miRNAs following tumor implantation and the transfer of exogenous miR-21 from the tumor to stromal cells. In this model, endogenous miR-21 is not expressed in stromal cells, so the presence of miR-21 should be exclusively derived from the implanted tumor cells. Three weeks after implantation, mice were euthanized, and brains were mechanically and enzymatically digested for subsequent fluorescence activated cell sorting (FACS) (**Fig. 2A**). Microglial cells were sorted based on the absence of RFP (black gate) and levels of CD11b and CD45 (blue gate)(Bennett et al., 2016). A carrier fluid injected (mock) brain was used to determine the GFP cut-off (red and green gate) (**Fig. 2B**). From tumor-bearing brain, microglial cells were isolated with the control GFP cut-off used to separate cells negative for GFP (red box; EV-GFP$^{neg}$) and positive for GFP (green box; EV-GFP$^{pos}$). The presence of GFP in microglia thus indicates tumor-derived EV uptake (**Fig. 2C**). The expression level of miR-21 was detected at significantly higher levels in microglia, which had taken up tumor EVs as compared to GFP-negative cells (**Fig. 2D**). The difference detected between mock microglia and EV-GFP$^{neg}$ microglia could be due to uptake of high-density lipoproteins, which carry some miR-21 (**Supplementary Fig. S2**).

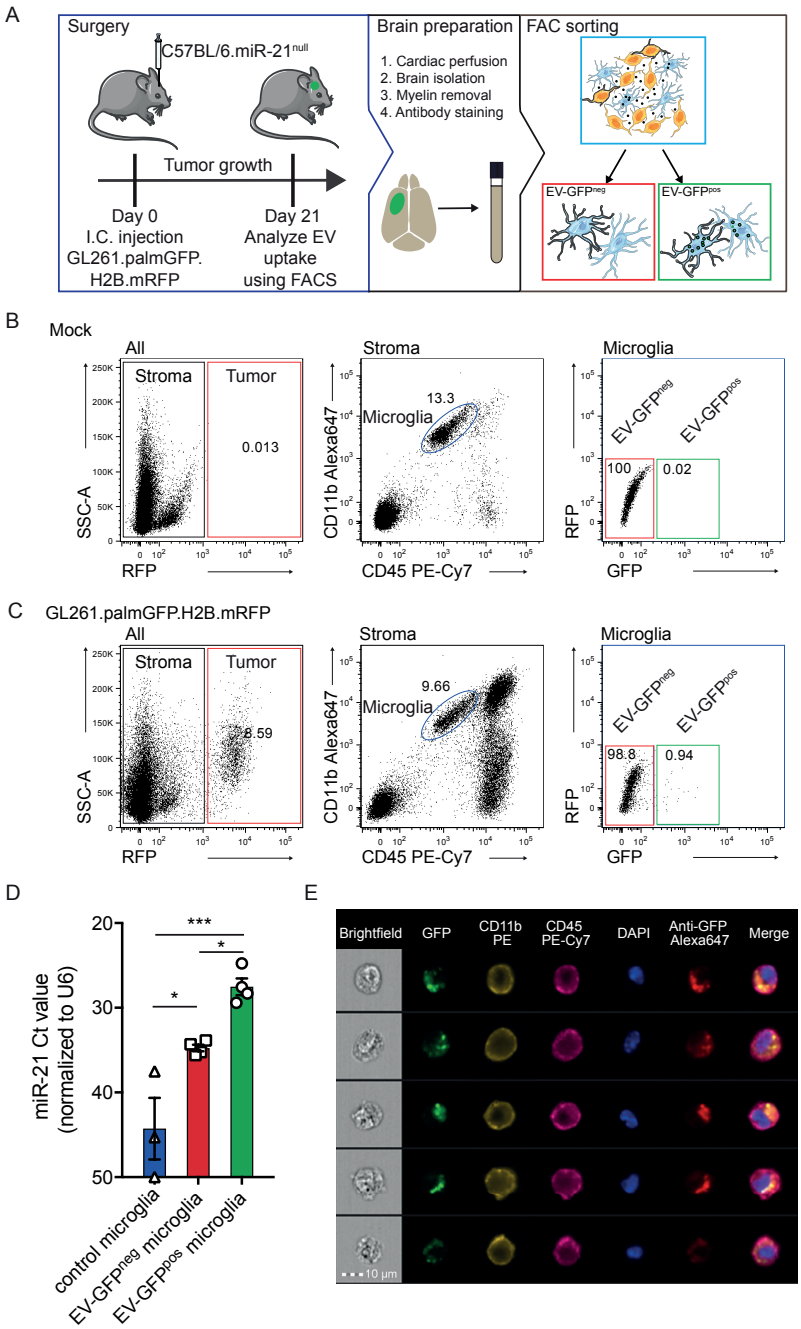


**Figure 2. miR-21 is transferred to microglia after uptake of tumor-derived EVs.** (**A**) Schematic illustration of experimental setup using C57BL/6.miR-21-null mice implanted with GL261.palmGFP.H2B.mRFP glioma cells that release palmGFP fluorescent EVs. Brains were harvested 21 days after implantation. Tissue was dissociated using enzymatic and mechanic digestion and microglia sorted based on cell markers and EV-GFP uptake. (**B**)

Representative FACS plots showing gating strategy where RFP expression is used to exclude tumor cells in downstream analysis and subsequently microglia were identified as CD11b$^{high}$/CD45$^{med}$ cells (blue gate). Microglia were then sorted based on the GFP signal detected as the upper limit in control (no tumor). (**C**) In mice implanted with GL261.palmGFP.H2B.mRFP, similar analysis (as in **B**) revealed a population of GFP-positive microglia (green gate in the microglia plot). (**D**) Uptake of EV-GFP results in the elevated levels of miR-21 in microglia, as compared to control microglia (blue), with Ct>40 considered baseline. (**E**) EV-GFP uptake visualized by imaging flow cytometry using ImageStream. Five representative cells presented showing EV-GFP co-localized with anti-GFP Alexa Fluor 647 within the contours of microglia as show by membrane marker CD11b and CD45. Scale bar 10 μm. Data represents 4 independent experiments and are presented as the mean with SEM (error bars). *P<0.05, **P<0.01. One-way ANOVA with Tukey's multiple comparisons test.

A similar trend between EV-GFP$^{neg}$ and EV-GFP$^{pos}$ microglia was seen in glioma-specific miR-10b, where the expression level was higher than in EV-GFP$^{neg}$ microglia (**Supplementary Fig. S1D**). Using a similar approach, MO/Mφ were identified by their high expression of CD45 and CD11b (blue gate as indicated in the figure legend)(Bennett et al., 2016), separating GFP-positive cells from GFP-negative cells (**Fig. 3A-B**). Similar to the microglial cells, an increased level of miR-21 was detected in EV-GFP$^{pos}$ MO/Mφ in comparison to EV-GFP$^{neg}$ cells (**Fig. 3C**). Surprisingly the difference between EV-GFP$^{neg}$ and GFP$^{pos}$ in MO/Mφ was smaller and the relative levels in EV-GFP$^{pos}$ MO/Mφ were lower when compared to EV-GFP$^{pos}$ microglia (**Fig. 2D and 3C**). To further validate that the GFP uptake is caused by EV-sized particles rather than phagocytosis of complete cells, ImageStream analysis was used to visualize the uptake of GFP in microglial cells and MO/Mφ (CD11b-PE, CD45-PE-Cy7 positive), using anti-GFP conjugated with Alexa Fluor 647 to exclude auto-fluorescence frequently encountered in myeloid cells and to confirm the uptake of GFP$^{pos}$ vesicle-like structures (**Fig. 2E and 3D**). This analysis, as expected, did confirm the presence of subcellular GFP positive particles in the microglial cells and MO/Mφ cells (**Fig. 2E and 3D**). To confirm if the transfer of GFP is associated with functional miR-21 transfers into microglia, the miR-21 levels in cells after EV uptake was examined (**Fig. 2D**). To further investigate to what extend EVs are taken up by other immune cells we quantified GFP uptake by CD11b$^{low}$CD45$^{high}$ lymphocytes (**Supplementary Fig. S3A**). In this population of non-phagocytic cells, we found a smaller percentage of cells that have taken up EV-GFP (**Supplementary Fig. S3A-B**). Moreover, the ImageStream and FACS analysis also allowed us to verify the expression of CD11b and CD45 on microglia and the absent of expression in tumor cells (**Supplementary Fig. S4A-D**). Taken together, this demonstrates that the combination of CD11b and CD45 can be used to isolate microglia and MO/Mφ cells and that GFP-positive EVs released by tumor cells *in vivo* can transfer miR-21 to microglia.

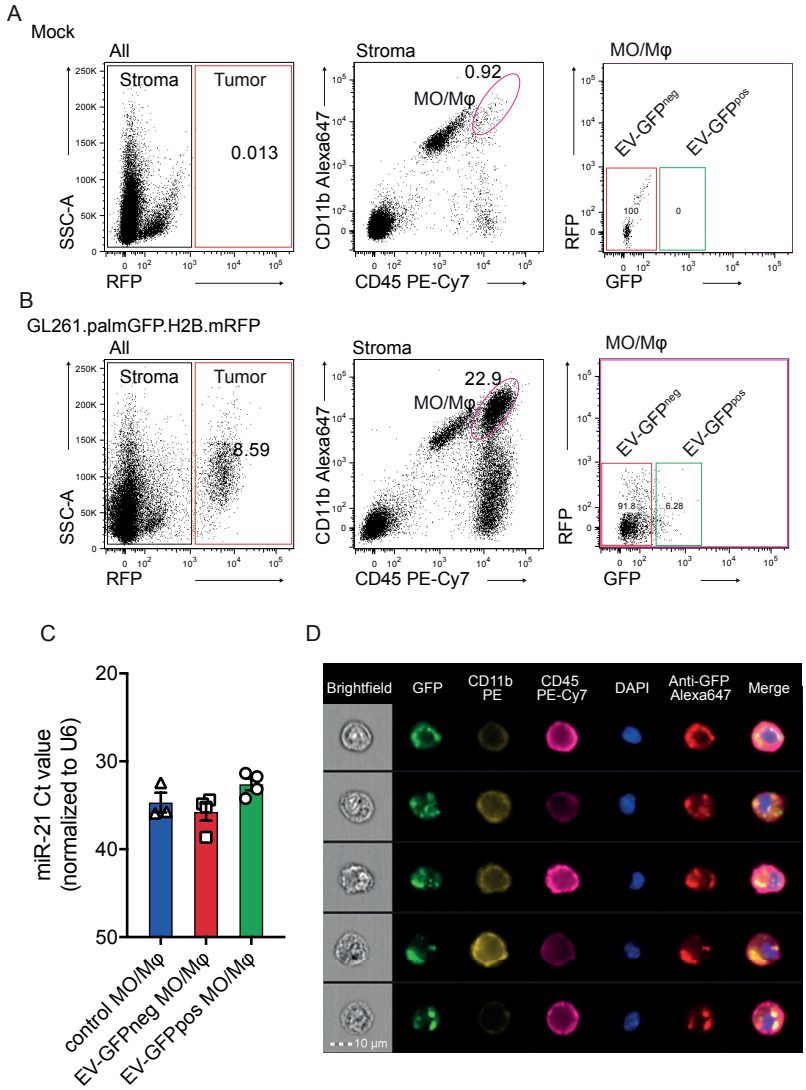


**Figure 3. miR-21 is transferred to monocytes/macrophages after uptake of tumor-derived EVs**. (**A**) Monocytes/macrophages (MO/Mφ) from miR-21-null mice were identified by FACS as CD11b$^{high}$/CD45$^{high}$ cells (magenta gate). MO/Mφ were then sorted based on the GFP signal detected as the upper limit in control (no tumor). (**B**) In mice implanted with GL261.palmGFP.H2B.mRFP, a population of GFP-positive MO/Mφ was identified (green gate in the GFP/RFP plot). (**C**) Uptake of EV-GFP resulted in the presence of miR-21 in MO/Mφ. (**D**) EV-GFP uptake was visualized by imaging flow cytometry using ImageStream. Scale bar 10 µm. Data represents 3 independent experiments and are presented as the mean with SEM (error bars). One-way ANOVA with Tukey's multiple comparisons test.

## *EV-mediated transfer of miR-21 leads to downregulation of specific mRNA targets in microglia*

One of the main functions of miR-21 is mRNA target cleavage, leading to reduction of levels of specific mRNAs. To study this, we analyzed the mRNA transcriptome of microglia, which were separated by FACS based on whether or not they contained EV-GFP. Unsupervised clustering of the top 750 most differentially expressed genes showed a clear distinction between microglia from control and tumor-bearing EV-GFP$^{neg}$ and EV-GFP$^{pos}$ microglia (**Fig. 4A**). To focus on the effect of the miR-21 transfer from tumor cells to microglia, the transcripts in EV-GFP$^{neg}$ and EV-GFP$^{pos}$ microglia were further analyzed. Four hundred and forty-one genes were significantly upregulated, and 359 genes were downregulated in EV-GFP$^{neg}$ versus EV-GFP$^{pos}$ (**Fig. 4B;** significantly changed genes in red). To further investigate miR-21 targets we derived a list of miR-21 targets by merging the results from two publicly available databases (miRTarBase and miRWalk)(Chou et al., 2018; Dweep and Gretz, 2015; Dweep et al., 2011), all references and evidence to miR-21 targets listed in the database were manually curated. To focus on validated targets rather than predicted targets, only genes from references showing direct downregulation of target genes based on luciferase assays, qPCR analyses or western blots were included (**Supplementary Table S1**). Relative gene expression of the selected 59 target genes showed 25 genes with a lowest expression in EV-GFP$^{pos}$ microglia (**Fig. 4C**). The genes with significantly reduced expression in the EV-GFP$^{pos}$ compared to EV-GFP$^{neg}$ microglia (p-adjusted (p-adj) < 0.05) include *Nfat5, Bmpr2, Btg2, Rhob* and *Kbtbd2* (**Fig. 4C**; significantly changed genes in bold). Interestingly, two genes (*FasL* and *Tgfbi)* regulated by miR-21 are expressed at a significantly higher level in EV-GFP$^{pos}$ compared to EV-GFP$^{neg}$ microglia (p-adj < 0.05) (**Fig. 4C**). Overall, these results demonstrate that the transfer of miR-21 by EVs *in vivo* results in downregulation of some of the miR-21 target mRNAs.

**Figure 4. miR-21 downregulates target mRNAs in tumor-associated microglia.** (**A**) In unsupervised clustering analysis, the top 750 most differentially expressed genes microglia clustered based on tumor status and EV-GFP uptake status. (**B**) MA-plot shows 441 significantly upregulated and 359 downregulated genes (plotted in red) when comparing EV-GFP$^{pos}$ to EV-GFP$^{neg}$ microglia. (**C**) Heatmap shows relative gene expression for 59 validated miR-21 gene targets. Bold gene names indicate genes with p-adj<0.05 in differential expression analysis EV-GFP$^{pos}$ versus EV-GFP$^{neg}$ microglia**.**

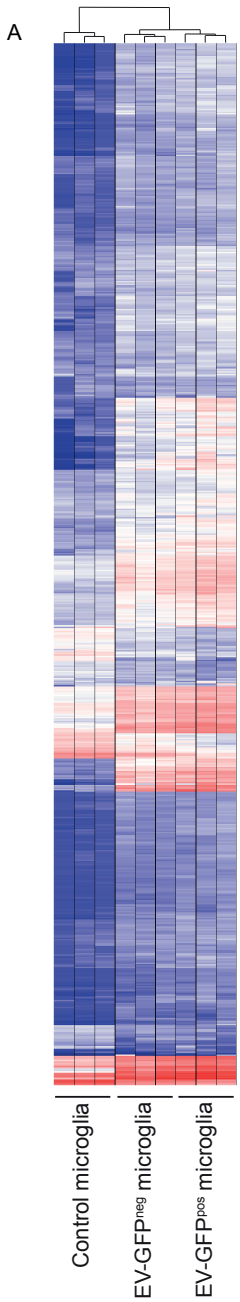
A
Control microglia
EV-GFPneg microglia
EV-GFPpos microglia

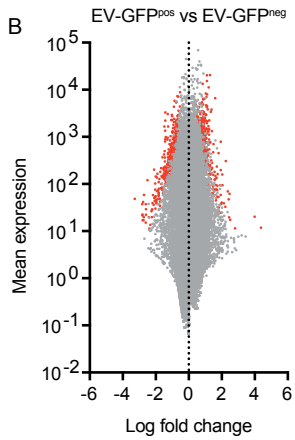
B
EV-GFPpos vs EV-GFPneg
Mean expression
Log fold change

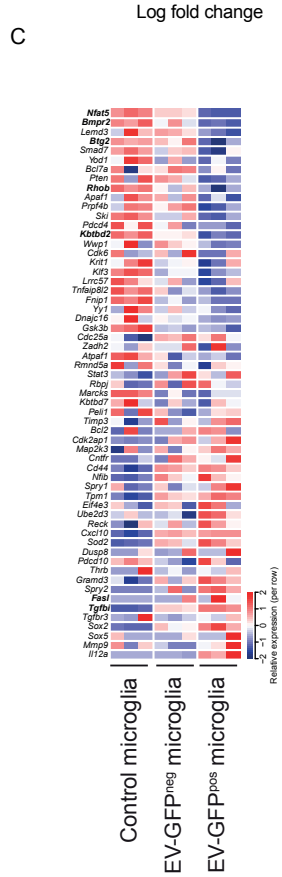
C
Nfat5
Bmpr2
Btg2
Rhob
Kbtbd2
Fasl
Tgfbi
Relative expression (per row)
Control microglia
EV-GFPneg microglia
EV-GFPpos microglia

## *miR-21 downregulates genes involved in cell proliferation in microglia*

While the selected mRNA targets (**Fig. 4C**), which are targets of miR-21 (**Supplementary Table S1**), are found in a variety of cell types, we set out to validate these targets in microglia *in vitro.* Cultures of primary microglia isolated from neonatal miR-21-null mice were transfected with a miR-21 mimic and a scrambled control RNA. Subsequently, the levels of the mRNA targets identified in the *in vivo* setting were tested by qRT-PCR. From the selected genes, expression level for *Btg2* and *Nfat5* as well as *Pdcd4* were significantly downregulated after EV uptake *in vivo*, were shown to be significantly downregulated by the miR-21 mimic (**Fig. 5A**). A control gene not targeted by miR-21, *Gapdh*, was not affected, as indication that mRNA target gene downregulation is miR-21 specific (**Fig. 5B**). In order to evaluate the effects of transfer of miR-21 by tumor-derived EVs to microglia *in vitro*, EVs from conditioned media (EV) and unconditioned media (UcM) (from cultures with and without GL261 cells, respectively) were isolated using a differential centrifugation protocol (**Fig. 5C**). Primary neonatal miR-21-null mouse microglia were then incubated with EVs and UcM. The microglia, 1 x $10^5$ cells, were exposed to a single dose of EVs, 2.43 x $10^{10}$ particles. Twenty-four hours later, the expression level of miR-21 was significantly increased in microglia exposed to GL261-derived EVs, as compared to UcM (**Fig. 5D**). We also observed a significant downregulation of the *in vivo* EV downregulated miR-21 targets *Bmpr2, Btg2, Kbtbd2, Pdcd4, Pten,* and *Rhob* transcripts, while the *Gapdh* expression appeared unaffected (**Fig. 5E-F**). Also, we tested whether microglia from wild type mice were also affected by the uptake of glioma derived EV in a similar way. We exposed primary neonatal wild type microglia to a single dose of EVs (2.43 x $10^{10}$ particles).

Expression levels of the miR-21 targets were analyzed 24 hours after EV exposure. Here we found similar trends of downregulation of the mRNA targets (**Supplementary Fig. S5A**). Using a similar approach as shown in Figure 2 we isolated microglia from a tumor bearing brain of a miR-21 expressing mouse and investigated the levels of miR-21 targets. We found similar patterns of downregulation of miR-21 targets in the miR-21 wild type mice compared to miR-21-null mice (**Supplementary Table S1, Supplementary Fig. S5B**). Taken together, these data demonstrate that miR-21 either introduced by transfection or delivered through EVs can downregulate specific mRNAs in miR-21-null and wild type microglia that were downregulated *in vitro* and *in vivo*.

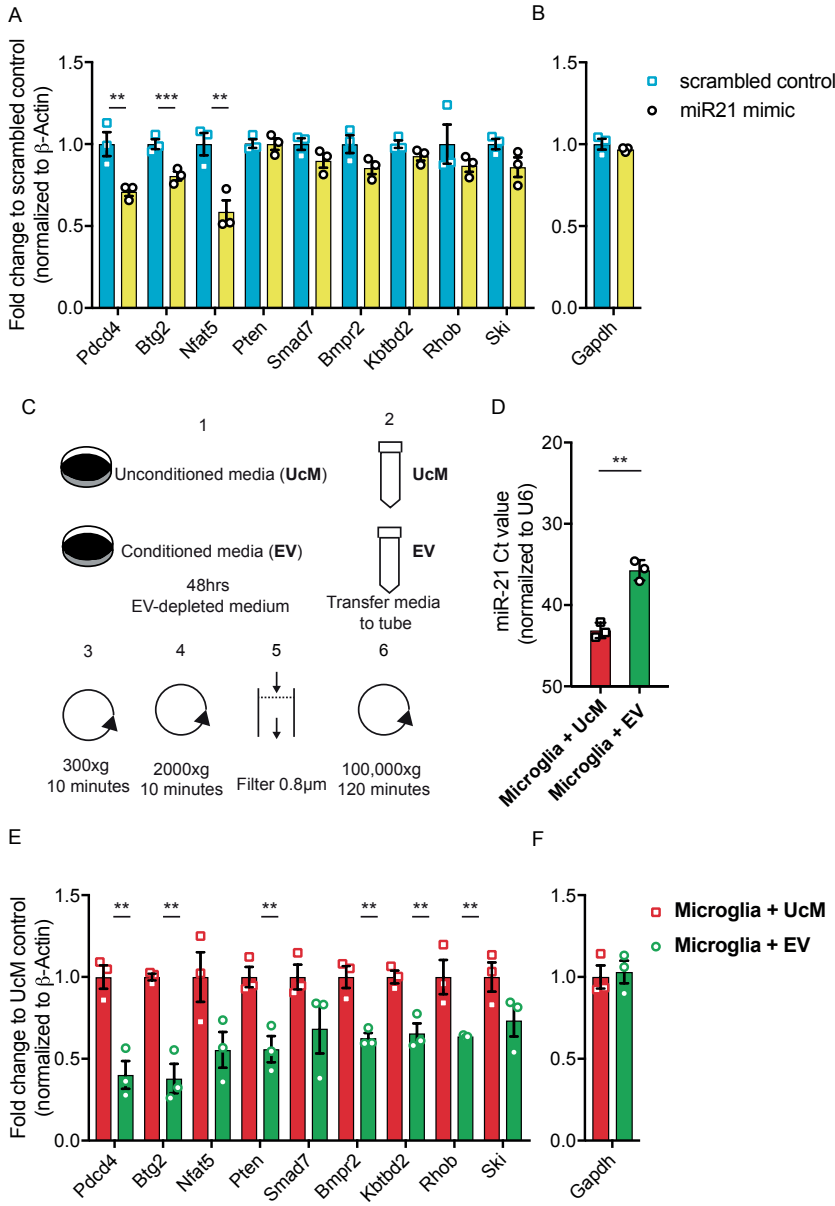


**Figure 5. miR-21 regulates selected target genes *in vitro* in primary neonatal microglia.** (**A**) In comparison to scrambled control, transfection of miR-21-mimic in primary neonatal miR-21-null mice microglia result in significant downregulation of miR-21 target genes (*Btg2, Nfat5* and *Pcdc4*) normalized to *β-Actin*. (**B**) Transfection of miR-21-mimic in primary neonatal miR-21-null mice microglia, did not affect a control gene *Gaphd*, (not targeted by miR-21), was shown not to be affected (**C**) Schematic overview of EV isolation using differential centrifugation. EVs from conditioned media cultured with GL261 cells (EV) and unconditioned media (UcM) were subjected to differential centrifugation. Collected EV pellet was resuspended in PBS and added to miR-21-null microglia. (**D**) EVs

from conditioned media (EV) and unconditioned media (UcM) were isolated and added to miR-21-null primary microglia followed by 24 hours incubation. Increased levels of miR-21 were detected in microglia exposed to GL261-derived EV, as compared to control media, with Ct>40 considered baseline. (**E**) Fold expression of miR-21 target genes (*Bmpr2, Btg2, Kbtbd2, Nfat5, Pdcd4, Pten, Rhob, Smad7 and Ski*) and (**F**) *Gapdh*, a gene not targeted by miR-21, normalized to *β-Actin* in miR-21-null microglia exposed to GL261-derived EVs, as compared to UcM. Data represents 3 independent experiments and are presented as the mean with SEM (error bars). **P<0.01, ***P<0.001. Unpaired T-test and multiple T-test

## *Intracranial delivery of GL261-derived EVs results in effective transfer of miR-21 in endogenous cells*

Our *in vitro* experiment showed that EV-mediated miR-21 transfer downregulates a select number of target mRNAs in microglia, hence it is important to evaluate whether this effect also occurs in an *in vivo* setting. By using EVs isolated from GL261, grown *in vitro,* we can study the uptake and effect of these EVs without confounding action of other factors released by the tumor cells. Using the previously described 100,000xg EV isolation protocol (**Fig. 1B**), we resuspended the GL261-derived EVs in PBS. A total of 1.26 x $10^9$ particles as measured by NTA were used. A carrier control (PBS) was used to set the cut-off of the GFP within the microglial population (blue circle and green box) (**Fig. 6A**). Sixteen hours after injection of the EVs into the left striatum (using similar coordinates as tumor implantation) of miR-21-null mice, about 0.3% of all microglia in the brain (blue circle) that had taken up EVs (green box) were detected (**Fig. 6B**). Interestingly, miR-21 was detected in the EV-GFP$^{pos}$ microglia, compared to being at non-detectable levels in EV-GFP$^{neg}$ microglia, demonstrating that miR-21 was effectively transferred via EVs derived from *in vitro* cultured tumor cells and delivered to microglia *in vivo* (**Fig. 6C**). This EV-uptake occurs soon after injection, as the EV-GFP signal was no longer detectable 40 hours after injection of EVs (data not shown), indicating the degradation of EV-GFP. *In vitro* experiments showed that levels of *Pdcd4* and *Btg2* were regulated by miR-21 in microglia (**Fig. 5A**) and were shown to be downregulated after exposure to glioma EVs (**Fig. 5D**). In this experiment both transcript levels were reduced in microglia that took up EV-GFP, however, this reduction reached significance only for the *Btg2* replicates (**Fig. 6D**). Interestingly, of the two targets only *Btg2* was among the initially downregulated miR-21 targets *in vivo*. The levels of miR-21 were lower in the microglia after EV-GFP uptake (delivered intracranially), compared to the tumor samples or microglia transfected *in vitro*. The relatively low levels of miR-21 in the EV-GFP brain injection experiment may explain the incomplete downregulation of the *Pdcd4* gene. However, these results suggest that in the absence of a tumor, microglia can take up tumor cell-derived EVs injected into the striatum leading to miR-21 dependent downregulation of *Btg2*.

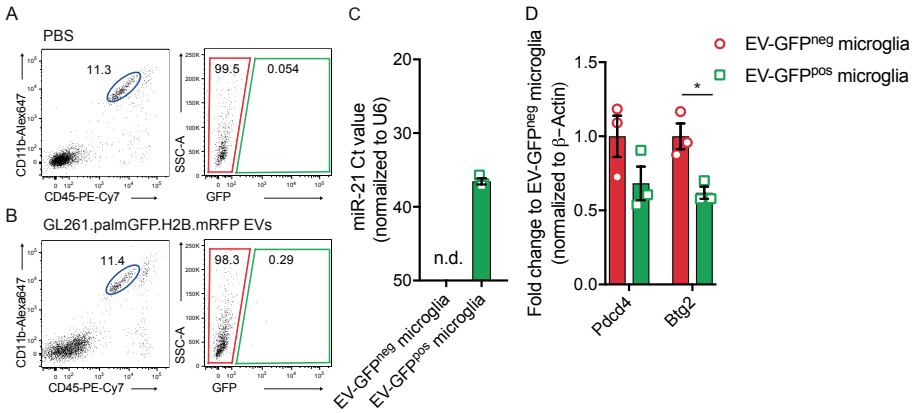


**Figure 6. EV-GFP uptake after EV intracranial injection** (**A**) PBS or (**B**) GL261.palmGFP.H2B.mRFP EVs were injected intracranially, after 16 hours brains were dissociated, and microglia were sorted based on EV-GFP uptake. (**C**) Uptake of EV-GFP resulted in elevated levels of miR-21 in microglia, levels in EV-GFP$^{neg}$ microglia were not detectable (n.d.), with Ct>40 considered baseline (**D**) Gene expression analyzed using ddPCR showing that *Pdcd4* and *Btg2* expression is reduced after EV-GFP uptake. Data represents 3 independent experiments and are presented as the mean with SEM (error bars). *P<0.05. Multiple T-test.

## *Btg2 downregulation leads to increased microglia proliferation*

A number of the downregulated genes, including Pdcd4 and Btg2, are involved in cellular proliferation. Pathway analysis of genes differentially expressed at higher levels in EV-GFPpos compared to EV-GFPneg microglia indeed showed that a number of pathways involved in cell cycle control were upregulated, indicating a higher degree of proliferation in microglia after EV uptake (Supplementary Fig. S6A). To test whether microglia have a higher degree of proliferation after EV uptake we analyzed the expression level of a number of genes that are described to be involved in microglial proliferation (Hammond et al., 2019). All of these genes are expressed at higher levels in microglia from tumor-bearing brains, with the highest expression in EV-GFPpos microglia (Fig. 7A). To further investigate the effect of miR-21 and Btg2 on microglial proliferation, we transfected miR-21 KO microglia with miR-21 mimic or siRNA against Btg2. Thereafter, the number of Ki67 positive cells was quantified comparing miR-21 mimic versus scrambled control and siRNA targeting Btg2 versus a siRNA control. Using a miR-21 mimic a higher number of microglia express the Ki67 proliferation marker after 24 hours of transfection (Fig. 7B-C). The downregulation of Btg2 after siRNA transfection also yielded a higher number of microglia expressing Ki67 (Fig. 7D-F). Overall, these results show that microglial proliferation is increased upon the delivery of miR-21 and after the downregulation of Btg2.

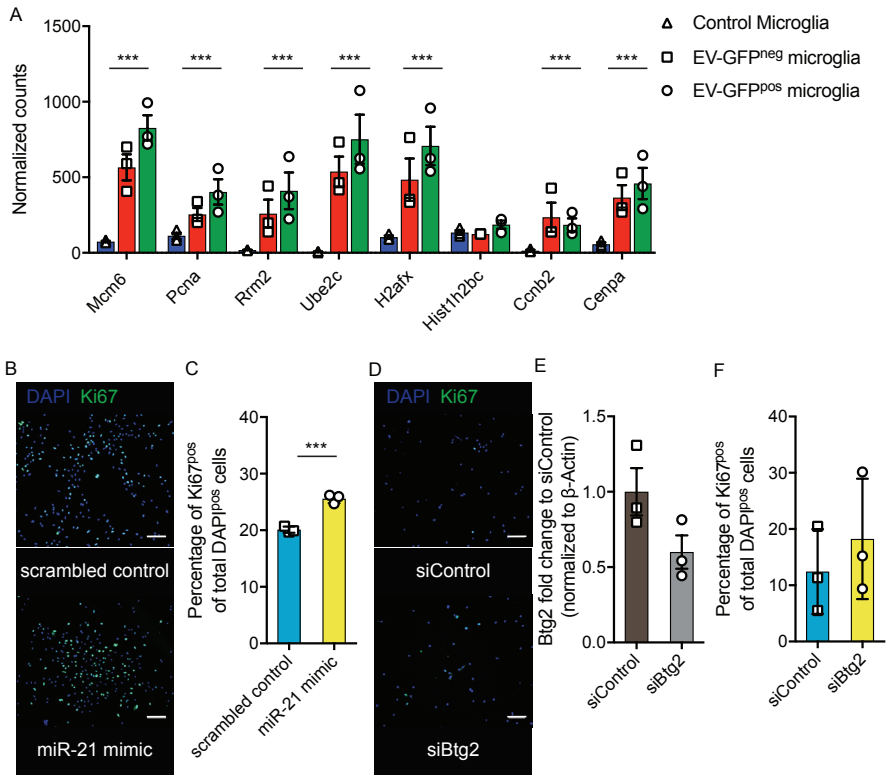


**Figure 7. *Btg2* downregulation leads to increased microglia proliferation.** (**A**) Normalized read count of genes involved in microglia proliferation (Hammond et al., 2019) (B) Representative images of in vitro culture miR-21-null microglia transfected with miR-21 mimic and control showing DAPI and Ki67 staining 24 hours after transfection. Scale bar 100 µm. (C) Quantification of proliferation 24 hours after transfection with miR-21 mimic or control as measured by Ki67 positive cells per total number of DAPI positive cells. (D) Representative images of in vitro culture miR-21-null microglia transfected with siRNA against Btg2 and siRNA control showing DAPI and Ki67 staining 24 hours after transfection. Scale bar 100 µm (E) Quantification of proliferation 24 hours after transfection with siRNA against Btg2 or control as measured by Ki67 positive cells per total number of DAPI positive cells. Data represents 3 independent experiments and are presented as the mean with SEM (error bars). ***P<0.001 multiple testing adjusted p-value differential expression in (A) and ***P<0.001. Unpaired T-test in (C, E-F).

## Discussion

EV-mediated miRNA transfer downregulates specific mRNAs *in vivo*. By using a palmitoylated fluorescent protein stably expressed in tumor cells we were able to track the uptake of tumor EVs by other cells in the brain(Lai et al., 2015; van der Vos et al., 2016). This reporter is not specific to one type of vesicles (e.g. exosomes, ectosomes or microvesicles)(Cocucci and Meldolesi, 2015), but follows the uptake

of all naturally formed membrane-bound vesicles. Microglia are known to be highly infiltrative into gliomas and we have shown that they avidly take up tumor-derived fluorescent EVs(van der Vos et al., 2016). Here we show that the cargo of the EVs is transferred into the microglia resulting in the delivery of functional miR-21.

In the current literature, EVs isolated after ultracentrifugation (100,000xg pellet) or smaller EVs isolated after size exclusion chromatography have been studied the most. We included the 2000xg pellet (mostly comprised of apoptotic bodies) in our analysis as well and even though we were able to detect miR-21 in these particles, we could not detect upregulation of miR-21 compared to cellular levels, as were found for the 100,000xg pellet. Additionally, by injecting the 2000xg pellet into non-tumor bearing mice, we only detected incidental GFP uptake by microglia indicating that the EVs isolated after ultracentrifugation are taken up to a greater extent microglial cells *in vivo*. Moreover, we found that miR-21 is also present in the high-density fractions by density gradient centrifugation (containing high-density lipoproteins), indicating that these may add to the EV mediated miR-21 transfer and could explain the presence of miR-21 in $GFP^{neg}$ microglia(Vickers et al., 2011). Overall, the cargo of the glioma-derived EV subtypes is transferred into the microglia resulting in the delivery of functional miR-21. Although EV mediated miRNA transfer was previously either shown *in vitro* or after injection of arbitrary amounts of highly subselected EVs *in vivo*, this study demonstrates *in vivo* functional transfer of miRNA by spontaneously released EVs.

Due to their high abundance in tumor tissue we focused in this study on the microglia and infiltrating MO/Mφ. Analysis of the EV-GFP uptake and the subsequent miR-21 levels in miR-21-null mice showed that while the percentage of cells positive for EV-GFP uptake was highest in the MO/Mφ population, the miR-21 transfer was most efficient in microglia. This could be due to differential uptake mechanisms, for example microglia have been known to take up EV through macropinocytosis while MO/Mφ use phagocytosis possibly followed by degradation(Fitzner et al., 2011). These differential uptake mechanisms can result in the difference of miR-21 level detected. So far, it has been reported that EVs derived from oligodendrocytes, glioma cells and neural stem cells are taken up by microglia(Fitzner et al., 2011; Morton et al., 2018; van der Vos et al., 2016). Within the developing brain the role of EVs in the communication between neural stem cells and neighboring microglia has also been shown to change the transcriptional state of the latter(Morton et al., 2018). Here, we used flow cytometry and image flow cytometry to visualize the uptake of fluorescently labeled EVs by microglia. By analyzing the transcriptome of the tumor associated miR-21-null microglia, we observed downregulation of miR-21 target mRNAs after uptake of tumor EVs. Overall, following uptake of the fluorescent EVs, miR-21 needs to exit the vesicles

to become functional. Upon release of miR-21 and palmGFP into the cytosol, the palmGFP might associate with other membranes in the cells and would probably be diluted out so as to be lost visually. Alternatively, a fraction of miR-21 and palmGFP might be retained in endosomes and degraded in late endosomes/lysosomes. Since the uptake of palmGFP EVs is most probably not a one-time but a continuous process, palmGFP and thus levels of miR-21 in cells may be in both the endosomes and cytosol/membranes. The downregulation of target mRNAs as we detected supports the notion that miR-21 is release into the cytosol after uptake of miR-21$^{+}$ tumor EVs. While other EV components, such as different small and large RNAs as well as proteins and lipids are also anticipated to affect microglia, we have, by making use of the miR-21-null mouse, been able to dissect the effects of the transfer of this single miRNA. Especially for *Btg2* we were able to show EV miR-21 mediated knockdown *in vivo* and were able to validate the role of EVs in additional *in vivo* and *in vitro* studies.

Here, we have demonstrated a mechanism through which a tumor can change the molecular profiles of microglia. EV-mediated transfer of miRNA from tumor cells to microglia results in downregulation of specific target genes. The gene that was most strikingly altered by EV mediated miR-21 transfer was *Btg2* (synonyms, *Pc3* and *Tis21*). This gene belongs to the BTG/Tob protein family which is comprised of 6 genes (*BTG1*, *BTG2/PC3/Tis21*, *BTG3/ANA*, *BTG4/PC3B*, *Tob1/Tob* and *Tob2*) and all are involved in the control of cellular proliferation and differentiation(Matsuda et al., 2001). *Btg2* negatively controls proliferation by reducing the activity of cyclin D1 which drives the cell cycle as shown in medulloblastoma cells(Farioli-Vecchioli et al., 2007) and by inhibiting cell cycle transition from G1 to S phase in fibroblasts(Guardavaccaro et al., 2000). Increased levels of proliferation in microglia have been reported in neuro-inflammation and traumatic brain injury, indicating that disruption of the CNS homeostasis as is also occurring during tumor growth can result in proliferation of microglia(Febinger et al., 2015; Pepe et al., 2017). By downregulation of *Btg2* through transfection with miR-21 mimic or siRNA specific to this message we showed an increased level of proliferation in microglia in culture. Within a tumor it is possible that by reducing the anti-proliferative effects of *Btg2* in tumor-supporting microglia, these cells will increase proliferation resulting in an increased influence on shaping the tumor microenvironment. In addition, it has also been shown that glioma cells exchange extracellular material suggesting that EV mediated miR-21 transfer can also increase glioma cell proliferation(Al-Nedawi et al., 2008; Skog et al., 2008).

In conclusion, the results of this study demonstrate that glioma cells can reprogram microglia in part by transferring miR-21 through EVs. Using the fluorescent palmitoylated EV reporter we have been able to study the uptake of naturally secreted EVs *in vivo*. Reviewing our data, we propose a model in which EVs

secreted by tumor cells function as miRNA carriers, which deliver molecules that change the transcriptome and subsequent proliferative capacities of microglia. This observation opens up new opportunities for therapy aimed at disrupting this form of communication between tumor cells and surrounding cells, including tumor-associated microglia. It is proof that miRNAs can be transferred by EVs to cells in the brain *in vivo* with functional consequences.



## Material and Methods

### Animals

All animal experiments were conducted under the oversight of the Massachusetts General Hospital Institution Animal Care and Use Committee. B6;129S6-MiR-21atm1Yoli/J (miR-21-null) mice were maintained with unlimited access to water and food under a 12-hour light/dark cycle(Ma et al., 2011). Male and female mice ranging from 12 - 14 weeks in age were randomly assigned to experimental groups. For RNA sequencing 3 mice were assigned per group. Injection of EVs was also done with 3 animals per group.

### Cell Culture

Mouse glioma cell-line GL261 (NCI Tumor Repository) was cultured at 37°C in a 5% $CO_2$ humidified incubator. Culture media was comprised of Roswell Park Memorial Institute (RPMI) 1640 with L-glutamine (Corning) supplemented with penicillin (100 units/ml), streptomycin (100 µg/ml) (P/S) (Corning) and 10% fetal bovine serum (FBS) (Gemini Bioproducts). Cells were tested for mycoplasma contamination (Mycoplasma PCR Detection Kit, abm G238) and found negative. Cells grown for EV isolation were cultured in media supplemented with 5% EV-depleted FBS. FBS was depleted from EVs by 16 hours of ultracentrifugation at 160,000xg.

### Microglia Culture

Mixed glial cultures were isolated from cerebral cortices of P1 to P4 mouse pups. Meninges were removed, and cortical cells were dissociated using 0.05% Trypsin/EDTA (Corning) followed by cell straining using 100 µm and 40 µm cell strainers. Cells were cultured in DMEM with 20% FBS, 1% P/S and 10 ng/ml M-CSF (Gibco) in poly-D-lysine (PDL; Sigma-Aldrich; 10 µg/ml) on pre-coated T-75 culture flasks for 10-15 days. Primary microglia were harvested from confluent mixed glial culture by gentle shaking on an orbital shaker for 30-60 min at 180 rpm and cultured in

the same medium(Tamashiro et al., 2012).

### Lentiviral Transduction Reporter

GL261 cells were stably transduced using a CSCW2 lentiviral vector(Sena-Esteves et al., 2004) encoding palmitoylated GFP (palmGFP), resulting in membrane localized GFP expression in cells and EVs released by these cells(Lai et al., 2015; McCabe and Berthiaume, 1999). A second transduction was performed to stably express the H2B.mRFP reporter (Addgene #18982, acquired from Dr. Thorsten Mempel, MGH)(Welm et al., 2008). Following transduction, cells were sorted for single cell cloning on the expression of both GFP and RFP. A clone with stable expression of both reporters was used for all experiments. For imaging of the cells, they were seeded on PDL (Sigma-Aldrich) coated glass coverslips and incubated for 48 hours. Cells were then washed in PBS and fixed using 4% paraformaldehyde (PFA; Electron Microscopy Sciences) in PBS. DAPI (1 µg/ml) (Thermo Fisher) staining was performed for 30 min at room temperature. Slides were washed for 10 min using PBS and mounted on microscopy slides using ProLong® Diamond Antifade Mountant (Thermo Fisher). Fluorescence microscopy images were acquired on the Zeiss Axio Imager M2 (Carl Zeiss).

### Proliferation assay

miR-21-null primary microglia were seeded at the density of 70,000 cells/well on coverslips coated with poly-D-lysine (PDL; Sigma-Aldrich; 10 µg/ml). Microglia were transfected using DharmaFECT (Dharmacon) transfection reagent in Opti-MEM (Gibco). miR-21 mimic and scrambled control were used at a concentration of 20 µM, siRNA against *Btg2* and siRNA control at 5 µM. Transfection mixes were incubated for 30 min before adding to the cells, which were subsequently incubated for 24 hours at 37°C. After incubation, microglia were washed in PBS for 5 min and fixed in 100% ice-cold methanol for 10 min. After fixation cells were washed two times in PBS for 5 min. Microglia were blocked in 5% BSA and 0.1% Triton X-100 (USB) in PBS (PBS-T) for 4 hours. Microglia were then incubated with the primary antibody Ki67 anti-rabbit (Abcam, 1:4000) at 4°C overnight. Microglia were washed three times in PBS-T for 5 min. Secondary antibody goat anti-rabbit (Invitrogen, 1:400) was diluted in PBS-T and incubated for 1 hour in dark at RT. Microglia were stained for DAPI (Thermo Fisher, 1 µg/ml) diluted in PBST and incubated for 5 min. Coverslips were transferred to microscope slides (Fisherbrand) on a droplet of mounting medium (Vectashield, Vector Labs). Fluorescence microscopy images were acquired on the Zeiss Axio Imager M2 (Carl Zeiss). Quantification of proliferation 24 hours was measured as Ki67 positive cells per total number of DAPI positive cells using Image J.

### Vesicle Isolation Including Iodixanol Density Gradient

The differential ultracentrifugation protocol consisted of subsequent centrifugation at 300xg for 10 min and 2000xg 10 min. Two-thousand xg pellet was collected and resuspended in PBS or RIPA buffer respectively for injection or western blot analysis. Supernatants were filtered through 0.8µm filter (Sigma) and centrifuged for 100,000xg (*k*-factor of 220.1) 120 min in Quick-Seal® Polypropylene Tubes (Beckman) using Type 70 Ti in Optima XE ultracentrifuge (Beckman) to pellet EVs. For EV exposure experiments and western blot analysis, pellets were resuspended in remaining supernatant supplemented with OptiMEM and concentrated by centrifugation at 100,000xg (*k*-factor of 190.7) for 120 min in Thinwall Polypropylene Tubes (Beckman) using MLS-50 Swinging-Bucket Rotor (Beckman) in an Optima Max-XP Ultracentrifuge. Final EV pellet was resuspended in DPBS for exposure experiment or RIPA buffer for western blot analysis.

Prior to western blot analysis cells and EVs were lysed in RIPA buffer with protease inhibitors (Sigma). Protein concentration was determined using Pierce BCA protein assay (Thermo Fisher) and equal amounts were loaded and resolved on 10% SDS-PAGE gel (Thermo Fisher). After transfer onto nitrocellulose membranes, samples were probed for GFP (Thermo Fisher, A-11120, 1:1000), GAPDH (Millipore, CB1001, 1:1000), TSG101 (Abcam, ab125011, 1:500), ALIX (Santa Cruz, sc-53538, 1:200) and Flotillin-1 (Abcam, ab133497, 1:500). ECL Anti-Rabbit IgG (Sigma) and ECL Anti-mouse IgG (Thermo Fisher) corresponding to the primary antibody were used as a secondary antibody.

For iodixanol density gradient the 100,000xg EV pellet was resuspended in 300 µl supernatant and mixed by adding 1 ml 60% cold iodixanol (OptiPrep Density Gradient Medium, Sigma D1556), the mixture was subsequently transferred to a Thinwall Polypropylene Tubes (Beckman). One layer of 500 µl of 40% and 30% iodixanol (diluted with 10x PBS and Milli-Q) were loaded on top of the 46% layer consisting EVs in the suspension of 60% iodixanol. The remaining volume was filled using 10% iodixanol. The density step-gradients were centrifuged at 156,000xg for 16 hours at 4°C in using an Optima Max-XP Ultracentrifuge. After 1 ml of the top layer was removed and 12 fractions of 250 µl were collected sequentially and numbered 1-12 from top to bottom. The different fractions were weighted determine density and used for western blot analysis and miRNA quantification.

For western blot analysis, 30 µl of each fraction was lysed in RIPA buffer with protease inhibitors (Sigma Aldrich). Protein concentrations were determined using Pierce BCA protein assay (Thermo Fisher) and equal amounts were loaded and resolved on 10% SDS-PAGE gel (Thermo Fisher). After transfer onto nitrocellulose

membranes, samples were probed for GFP (Thermo Fisher, A-11122, 1:1000). ECL Anti-Rabbit IgG (Sigma) was used as secondary antibody corresponding to the primary antibody. The remaining volumes were used for RNA isolation and miRNA RT-qPCR quantification.

### Intracranial Tumor Injection

Adult miR-21-null mice were first anesthetized using 2.5% isoflurane in 100% oxygen via a nose cone. The left striatum was then either injected with 1 x $10^5$ cells of GL261.palmGFP.H2B.mRFP (GL261.pGHR) suspended in 2 µl OptiMEM or OptiMEM alone. Using a stereotactic frame, the cells were implanted at three coordinates from bregma: 0.5 mm left, 2 mm anterior and a depth of 2.5 mm from the skull. Three weeks after implantation, the mice were anesthetized with 120 µl of a mixture of ketamine (17.5 mg/ml) and xylazine (2.5 mg/ml) followed by transcardial perfusion with 50 ml cold Dulbecco's phosphate-buffered saline (DPBS) without magnesium and calcium for subsequent FACS using a perfusion pump (Minipump Variable Flow, Fisher Scientific).

### Tissue Digestion

Neural Tissue Dissociation Kit (P) (Miltenyi Biotec) was used to process the brain into a single cell suspension. Brains were placed into a GentleMacs™ C-tube (Miltenyi Biotec) with 1.9 ml Buffer X with 50 µl Neural Buffer P. Brain was dissociated using the gentleMACS Dissociator (Miltenyi Biotec) on the brain program settings, according to manufacturer's protocol. Myelin removal was achieved using magnetic separation together with anti-myelin beads (Miltenyi Biotec). The final cell suspension was re-suspended in 1X DPBS without calcium ($Ca^{2+}$) or magnesium ($Mg^{2+}$) (Corning) supplemented with 2 mM EDTA (Thermo Fisher) and 0.5% BSA (Sigma) following cell staining and FACS.

### Flow Cytometry Preparation

Non-specific binding of the immunoglobulin to the Fc receptors was blocked by incubating cells 10 min on ice in 0.5% BSA in DPBS (without $Ca^{2+}$ or $Mg^{2+}$) with 2 mM EDTA supplemented with TruStain fcX™ (anti-mouse Cd16/32, BioLegend, #101319, clone 93, 1:100). Cells were stained with anti-CD11B-Alexa647 (clone M1/70, 1:100) and anti-CD45-PE-Cy7 (clone 30-F11, 1:100) for 30 min on ice. Finally, cells were washed with 1 ml DPBS (without $Ca^{2+}$ or $Mg^{2+}$) with 0.5% BSA and 2 mM EDTA and were centrifuged at 300 × g for 10 min, resuspended in 0.5% BSA, 2 mM EDTA in DPBS (without $Ca^{2+}$ or $Mg^{2+}$) and passed through a 35 µm nylon mesh strainer (BD Falcon). DAPI was added to cells at final concentration

of 1 µg/ml. Live cells were sorted using a BD FACSAria II SORP Cell Sorter. Sorted cells were directly lysed in RLT Plus buffer (Qiagen) and RNA was extracted using the RNeasy Plus RNA isolation kit (Qiagen) according to manufactures protocol following appendix D.



### Image Stream Analysis

Following protocol described above to dissociate cells from the whole brain, cells were stained as listed above with anti-CD11B-PE (clone M1/70, 1:100) and anti-CD45-PE-Cy7. After staining, cells were fixed and permeabilized with BD Cytofix/Cytoperm™ following manufacturing protocol. After fixation and permeabilization cells were stained with anti-GFP-Alexa Fluor 647 (clone FM264G, 1:100) and DAPI to a final concentration of 1µg/ml. Flow imaging was done using Amnis ImageStream mkII Imaging Flow Cytometer.

### Intracranial Injection of EVs

Isolation of EV was done from conditioned media after 48 hours of culturing GL261 in RPMI with 1% P/S and 5% EV-depleted FBS (see "Cell Culture"). The differential ultracentrifugation protocol consisted of subsequent centrifugation at 300xg for 10 min and 2000xg 10 min. Supernatants were filtered through 0.8µm filter (Sigma) and centrifuged for 100,000xg (*k*-factor of 220.1) 120 min in Quick-Seal® Polypropylene Tubes (Beckman) using Type 70 Ti in Optima XE ultracentrifuge (Beckman) to pellet EVs. To wash and concentrate EVs, pellets were resuspended in remaining supernatant supplemented with OptiMEM and concentrated by centrifugation at 100,000xg (*k*-factor of 190.7) for 120 min in Thinwall Polypropylene Tubes (Beckman) using MLS-50 Swinging-Bucket Rotor (Beckman) in an Optima Max-XP Ultracentrifuge. Final EV pellet was resuspended in DPBS and characterization of EVs was performed by size distribution analysis using nanoparticle-tracking analysis (NTA 3.2; Malvern), with screen gain set at 3.0 and camera level at 13.0.

Following procedures as described in intracranial tumor implantation method section EVs or an equal volume of carrier fluid (PBS) was injected intracranially. Microglia were isolated 16 and 40 hours after injection of EVs or DPBS following procedures, as previously described.

### RT-qPCR

cDNAs for gene expression analysis with RT-qPCR were prepared using the SuperScript VILO cDNA Synthesis Kit (Invitrogen). qPCR mix was prepared

following manufacturing protocol of Power SYBR Green PCR Master Mix (Applied Biosystems). qPCR was performed using the QuantStudio 3 PCR system (Applied Biosystems). The cycling conditions used were 50°C for 2 min, 95°C for 10 min, and 40 cycles of 95°C for 15 sec and 60°C for 1 min following dissociation analysis. All qPCR reactions were done in triplicate and normalized to ß-Actin mRNA levels.

miRNA expression analysis was performed using miRCURY LNA miRNA PCR kit following manufacturing's protocol. miRNA expression was normalized to *U6* or UniSP6 spike-in RNA as listed in figure legends.

### Digital Droplet PCR (ddPCR)

To evaluate gene expression of from cells isolated after intracranial injection of EVs, cDNA was prepared using the SuperScript VILO cDNA Synthesis Kit (Invitrogen). Gene expression was analyzed using ddPCR following PrimePCR ddPCR Gene Expression Probe Assay. Using protocol as listed by manufacturer droplets were generated with DG8 Cartridge using QX200 droplet generator (Bio-Rad) and PCR performed with thermal cycling conditions as described. QX200 Droplet Reader and QuantaSoft Software (Bio-Rad) were used to analyze the gene expression.

### RNA Sequencing

The RNA concentration and integrity (RIN score) were determined using the Agilent 2100 Bioanalyzer Pico-chips (Agilent Technologies) following manufacturing protocol. RNA libraries were prepared with poly(A) selection using 3'-SMART CDS Primer II A within the SMARTer Ultra Low Input RNA Kit for Sequencing–v3 (Clontech Takara) following manufacturer's protocol including ERCC RNA Spike-In Mix (Life Technologies). Following first strand synthesis, cDNA was purified with 1x Agencourt AMPure XP beads (Beckman Coulter), as described in SMARTer protocol. Nextera® XT DNA Library Preparation kit (Illumina) was used for sample barcoding and fragmentation according to the manufacturer's protocol. Library amplification and library barcoding were achieved within 12 cycles of PCR. Subsequent PCR products were purified with 1.8x Agencourt AMPure XP beads according Nextera XT protocol. Library quantification was done using the SYBR® FAST Universal qPCR Kit (KAPA Biosystems). Equal molar individual libraries were pooled, and the pool concentration was determined using the KAPA SYBR® FAST Universal qPCR Kit. Finally, libraries were diluted and denatured with the addition of 1% PhiX Sequencing Control V3 (Illumina). 75-bp paired-end reads were generated using NextSeq 500/550 High Output v2 kit (150 cycles) on an Illumina NextSeq (Illumina).

### Data Processing and Analysis

Raw sequencing data were processed by aligning to the mm10 genome using the STAR v2.4.0h aligner, and removing duplicate using the MarkDuplicates (picard-tools-1.8.4). Read counts were generated with Gencode's GRCm38.p3 GTF annotations as reference using htseq-count.

After aligning and read counting, the downstream analysis was performed using the DESeq2 (version 1.10)(Love et al., 2014) in R (version 3.2.3). Differential expression analysis as performed in DESeq2 was subjected to statistical significance using Benjamini and Hochberg multiple testing adjusted p-values. The regularized logarithm (rlog) values were used for unsupervised clustering of top 750 most differential expressed genes between samples and to plot heatmaps using the gplots (version 2.17) heatmap.2 function in R.

Pathway analysis was performed in MetaCore using differential expression values between EV-GFP$^{pos}$ versus EV-GFP$^{neg}$ as generated in DESeq2. A cut-off value of significance of multiple testing adjusted p-value <0.05 was used to include differentially expressed genes.

Bar graph and MA plots were generated in GraphPad Prism (version 7.0c). Error bars display mean ±standard error of the mean (SEM). Significance was calculated using unpaired T-test, multiple T-tests and One-way ANOVA with Tukey's multiple comparisons test, with statistical significance defined as $p<0.05$.

### Data and Software Availability

Raw and processed transcriptomic data described in this manuscript are deposited in NCBI's Gene Expression Omnibus (GEO) and are accessible using GEO Series accession number GSE12607 at https://www.ncbi.nlm.nih.gov/geo/query/acc.cgi?acc=GSE126073.
All R scripts written for data processing are available online in a git repository. The files and information can be accessed at: https://github.com/slnmaas/miR21-Project.

## References

Abels, E.R., Broekman, M.L., Breakefield, X.O., and Maas, S.L. (2019). Glioma EVs Contribute to Immune Privilege in the Brain. Trends in Cancer.

Afonso, M.B., Rodrigues, P.M., Simão, A.L., Gaspar, M.M., Carvalho, T., Borralho, P., Bañales, J.M., Castro, R.E., and Rodrigues, C.M.P. (2018). miRNA-21 ablation protects against liver injury and necroptosis in cholestasis. Cell

Death Differ *25*, 857-872.
Ahmed, M.I., Mardaryev, A.N., Lewis, C.J., Sharov, A.A., and Botchkareva, N.V. (2011). MicroRNA-21 is an important downstream component of BMP signalling in epidermal keratinocytes. J Cell Sci *124*, 3399-3404.
Akers, J.C., Gonda, D., Kim, R., Carter, B.S., and Chen, C.C. (2013). Biogenesis of extracellular vesicles (EV): exosomes, microvesicles, retrovirus-like vesicles, and apoptotic bodies. J Neurooncol *113*, 1-11.
Al-Nedawi, K., Meehan, B., Micallef, J., Lhotak, V., May, L., Guha, A., and Rak, J. (2008). Intercellular transfer of the oncogenic receptor EGFRvIII by microvesicles derived from tumour cells. Nat Cell Biol *10*, 619-624.
Belter, A., Rolle, K., Piwecka, M., Fedoruk-Wyszomirska, A., Naskręt-Barciszewska, M.Z., and Barciszewski, J. (2016). Inhibition of miR-21 in glioma cells using catalytic nucleic acids. Sci Rep *6*, 24516.
Bennett, M.L., Bennett, F.C., Liddelow, S.A., Ajami, B., Zamanian, J.L., Fernhoff, N.B., Mulinyawe, S.B., Bohlen, C.J., Adil, A., Tucker, A.*, et al.* (2016). New tools for studying microglia in the mouse and human CNS. Proceedings of the National Academy of Sciences of the United States of America *113*, E1738-1746.
Bowman, R.L., Klemm, F., Akkari, L., Pyonteck, S.M., Sevenich, L., Quail, D.F., Dhara, S., Simpson, K., Gardner, E.E., Iacobuzio-Donahue, C.A.*, et al.* (2016). Macrophage Ontogeny Underlies Differences in Tumor-Specific Education in Brain Malignancies. Cell reports *17*, 2445-2459.
Broekman, M.L., Maas, S.L.N., Abels, E.R., Mempel, T.R., Krichevsky, A.M., and Breakefield, X.O. (2018). Multidimensional communication in the microenvirons of glioblastoma. Nat Rev Neurol *14*, 482-495.
Chan, J.A., Krichevsky, A.M., and Kosik, K.S. (2005). MicroRNA-21 is an antiapoptotic factor in human glioblastoma cells. Cancer Res *65*, 6029-6033.
Chen, H., and Boutros, P.C. (2011). VennDiagram: a package for the generation of highly-customizable Venn and Euler diagrams in R. BMC Bioinformatics *12*, 35.
Chen, X., Song, M., Chen, W., Dimitrova-Shumkovska, J., Zhao, Y., Cao, Y., Song, Y., Yang, W., Wang, F., Xiang, Y.*, et al.* (2016). MicroRNA-21 Contributes to Liver Regeneration by Targeting PTEN. Med Sci Monit *22*, 83-91.
Chou, C.-H., Shrestha, S., Yang, C.-D., Chang, N.-W., Lin, Y.-L., Liao, K.-W., Huang, W.-C., Sun, T.-H., Tu, S.-J., Lee, W.-H.*, et al.* (2018). miRTarBase update 2018: a resource for experimentally validated microRNA-target interactions. Nucleic Acids Res *46*, D296-D302.
Cocucci, E., and Meldolesi, J. (2015). Ectosomes and exosomes: shedding the confusion between extracellular vesicles. Trends in Cell Biology *25*, 364-372.
Conway, J.R., Lex, A., and Gehlenborg, N. (2017). UpSetR: An R Package for the Visualization of Intersecting Sets and their Properties. Bioinformatics.
Corsten, M.F., Miranda, R., Kasmieh, R., Krichevsky, A.M., Weissleder, R., and Shah, K. (2007). MicroRNA-21 knockdown disrupts glioma growth in vivo and displays synergistic cytotoxicity with neural precursor cell delivered S-TRAIL in human gliomas. Cancer Res *67*, 8994-9000.
de Vrij, J., Maas, S.L., Kwappenberg, K.M., Schnoor, R., Kleijn, A., Dekker, L., Luider, T.M., de Witte, L.D., Litjens, M., van Strien, M.E.*, et al.* (2015). Glioblastoma-derived extracellular vesicles modify the phenotype of monocytic cells. Int J Cancer *137*, 1630-1642.
Dobin, A., Davis, C.A., Schlesinger, F., Drenkow, J., Zaleski, C., Jha, S., Batut, P., Chaisson, M., and Gingeras, T.R. (2013). STAR: ultrafast universal RNA-seq aligner. Bioinformatics *29*, 15-21.
Dweep, H., and Gretz, N. (2015). miRWalk2.0: a comprehensive atlas of microRNA-target interactions. Nat Methods *12*, 697-697.
Dweep, H., Sticht, C., Pandey, P., and Gretz, N. (2011). miRWalk--database: prediction of possible miRNA binding sites by "walking" the genes of three genomes. J Biomed Inform *44*, 839-847.
El Fatimy, R., Subramanian, S., Uhlmann, E.J., and Krichevsky, A.M. (2017). Genome Editing Reveals Glioblastoma Addiction to MicroRNA-10b. Mol Ther *25*, 368-378.
Farioli-Vecchioli, S., Tanori, M., Micheli, L., Mancuso, M., Leonardi, L., Saran, A., Ciotti, M.T., Ferretti, E., Gulino, A., Pazzaglia, S.*, et al.* (2007). Inhibition of medulloblastoma tumorigenesis by the antiproliferative and pro-differentiative gene PC3. FASEB J *21*, 2215-2225.

Febinger, H.Y., Thomasy, H.E., Pavlova, M.N., Ringgold, K.M., Barf, P.R., George, A.M., Grillo, J.N., Bachstetter, A.D., Garcia, J.A., Cardona, A.E.*, et al.* (2015). Time-dependent effects of CX3CR1 in a mouse model of mild traumatic brain injury. J Neuroinflammation *12*, 154.

Fiorentino, L., Cavalera, M., Mavilio, M., Conserva, F., Menghini, R., Gesualdo, L., and Federici, M. (2013). Regulation of TIMP3 in diabetic nephropathy: a role for microRNAs. Acta Diabetol *50*, 965-969.

Fitzner, D., Schnaars, M., van Rossum, D., Krishnamoorthy, G., Dibaj, P., Bakhti, M., Regen, T., Hanisch, U.-K., and Simons, M. (2011). Selective transfer of exosomes from oligodendrocytes to microglia by macropinocytosis. J Cell Sci *124*, 447-458.

Fujita, S., Ito, T., Mizutani, T., Minoguchi, S., Yamamichi, N., Sakurai, K., and Iba, H. (2008). miR-21 Gene expression triggered by AP-1 is sustained through a double-negative feedback mechanism. J Mol Biol *378*, 492-504.

Gabriely, G., Wurdinger, T., Kesari, S., Esau, C.C., Burchard, J., Linsley, P.S., and Krichevsky, A.M. (2008). MicroRNA 21 promotes glioma invasion by targeting matrix metalloproteinase regulators. Mol Cell Biol *28*, 5369-5380.

Gao, X., Li, X., Qian, C., Li, F., Zhang, Y., Dang, L., Xiao, X., Liu, F., Li, H., and Zhang, X. (2016). MiR-21 functions oppositely in proliferation and differentiation of neural stem/precursor cells via regulating AKT and GSK-3β. Cell Mol Biol (Noisy-le-grand) *62*, 144-149.

Guardavaccaro, D., Corrente, G., Covone, F., Micheli, L., D'Agnano, I., Starace, G., Caruso, M., and Tirone, F. (2000). Arrest of G(1)-S progression by the p53-inducible gene PC3 is Rb dependent and relies on the inhibition of cyclin D1 transcription. Mol Cell Biol *20*, 1797-1815.

Hambardzumyan, D., Gutmann, D.H., and Kettenmann, H. (2016). The role of microglia and macrophages in glioma maintenance and progression. Nature Neuroscience *19*, 20-27.

Hatley, M.E., Patrick, D.M., Garcia, M.R., Richardson, J.A., Bassel-Duby, R., van Rooij, E., and Olson, E.N. (2010). Modulation of K-Ras-dependent lung tumorigenesis by MicroRNA-21. Cancer cell *18*, 282-293.

He, X., Zhang, K., Gao, X., Li, L., Tan, H., Chen, J., and Zhou, Y. (2016). Rapid atrial pacing induces myocardial fibrosis by down-regulating Smad7 via microRNA-21 in rabbit. Heart Vessels *31*, 1696-1708.

Hu, B., Wang, X., Hu, S., Ying, X., Wang, P., Zhang, X., Wang, J., Wang, H., and Wang, Y. (2017). miR-21-mediated Radioresistance Occurs via Promoting Repair of DNA Double Strand Breaks. J Biol Chem *292*, 3531-3540.

Hu, S.-J., Ren, G., Liu, J.-L., Zhao, Z.-A., Yu, Y.-S., Su, R.-W., Ma, X.-H., Ni, H., Lei, W., and Yang, Z.-M. (2008). MicroRNA expression and regulation in mouse uterus during embryo implantation. J Biol Chem *283*, 23473-23484.

Johnston, D.G.W., Kearney, J., Zasłona, Z., Williams, M.A., O'Neill, L.A.J., and Corr, S.C. (2017). MicroRNA-21 Limits Uptake of Listeria monocytogenes by Macrophages to Reduce the Intracellular Niche and Control Infection. Front Cell Infect Microbiol *7*, 201.

Kölling, M., Kaucsar, T., Schauerte, C., Hübner, A., Dettling, A., Park, J.-K., Busch, M., Wulff, X., Meier, M., Scherf, K.*, et al.* (2017). Therapeutic miR-21 Silencing Ameliorates Diabetic Kidney Disease in Mice. Mol Ther *25*, 165-180.

Kowal, J., Arras, G., Colombo, M., Jouve, M., Morath, J.P., Primdal-Bengtson, B., Dingli, F., Loew, D., Tkach, M., and Théry, C. (2016). Proteomic comparison defines novel markers to characterize heterogeneous populations of extracellular vesicle subtypes. Proceedings of the National Academy of Sciences of the United States of America *113*, E968-977.

Krichevsky, A.M., and Gabriely, G. (2009). miR-21: a small multi-faceted RNA. J Cell Mol Med *13*, 39-53.

Kumarswamy, R., Volkmann, I., and Thum, T. (2011). Regulation and function of miRNA-21 in health and disease. RNA Biol *8*, 706-713.

Lai, C.P., Kim, E.Y., Badr, C.E., Weissleder, R., Mempel, T.R., Tannous, B.A., and Breakefield, X.O. (2015). Visualization and tracking of tumour extracellular vesicle delivery and RNA translation using multiplexed reporters. Nature Communications *6*, 7029.

Li, Q., and Barres, B.A. (2018). Microglia and macrophages in brain homeostasis and disease. Nature reviews Immunology *18*, 225-242.

Li, Q., Zhang, D., Wang, Y., Sun, P., Hou, X., Larner, J., Xiong, W., and Mi, J. (2013). MiR-21/Smad 7 signaling determines TGF-β1-induced CAF formation. Sci Rep *3*, 2038.

Li, W., and Graeber, M.B. (2012). The molecular profile of microglia under the influence of glioma. Neuro-oncology *14*, 958-978.

Liang, H., Zhang, C., Ban, T., Liu, Y., Mei, L., Piao, X., Zhao, D., Lu, Y., Chu, W., and Yang, B. (2012). A novel reciprocal loop between microRNA-21 and TGFβRIII is involved in cardiac fibrosis. Int J Biochem Cell Biol *44*, 2152-2160.

Liu, C., Li, B., Cheng, Y., Lin, J., Hao, J., Zhang, S., Mitchel, R.E.J., Sun, D., Ni, J., Zhao, L.*, et al.* (2011). MiR-21 plays an important role in radiation induced carcinogenesis in BALB/c mice by directly targeting the tumor suppressor gene Big-h3. Int J Biol Sci *7*, 347-363.

Lorenzen, J.M., Schauerte, C., Hübner, A., Kölling, M., Martino, F., Scherf, K., Batkai, S., Zimmer, K., Foinquinos, A., Kaucsar, T.*, et al.* (2015). Osteopontin is indispensible for AP1-mediated angiotensin II-related miR-21 transcription during cardiac fibrosis. Eur Heart J *36*, 2184-2196.

Love, M.I., Huber, W., and Anders, S. (2014). Moderated estimation of fold change and dispersion for RNA-seq data with DESeq2. Genome Biol *15*, 550.

Lu, T.X., Munitz, A., and Rothenberg, M.E. (2009). MicroRNA-21 is up-regulated in allergic airway inflammation and regulates IL-12p35 expression. Journal of immunology (Baltimore, Md : 1950) *182*, 4994-5002.

Lu, Z., Liu, M., Stribinskis, V., Klinge, C.M., Ramos, K.S., Colburn, N.H., and Li, Y. (2008). MicroRNA-21 promotes cell transformation by targeting the programmed cell death 4 gene. Oncogene *27*, 4373-4379.

Luo, X., Gu, J., Zhu, R., Feng, M., Zhu, X., Li, Y., and Fei, J. (2014). Integrative analysis of differential miRNA and functional study of miR-21 by seed-targeting inhibition in multiple myeloma cells in response to berberine. BMC Syst Biol *8*, 82.

Ma, X., Kumar, M., Choudhury, S.N., Becker Buscaglia, L.E., Barker, J.R., Kanakamedala, K., Liu, M.-F., and Li, Y. (2011). Loss of the miR-21 allele elevates the expression of its target genes and reduces tumorigenesis. Proceedings of the National Academy of Sciences of the United States of America *108*, 10144-10149.

Maas, S.L.N., Breakefield, X.O., and Weaver, A.M. (2017). Extracellular Vesicles: Unique Intercellular Delivery Vehicles. Trends in Cell Biology *27*, 172-188.

Marquez, R.T., Wendlandt, E., Galle, C.S., Keck, K., and McCaffrey, A.P. (2010). MicroRNA-21 is upregulated during the proliferative phase of liver regeneration, targets Pellino-1, and inhibits NF-kappaB signaling. Am J Physiol Gastrointest Liver Physiol *298*, G535-541.

Mateescu, B., Kowal, E.J.K., van Balkom, B.W.M., Bartel, S., Bhattacharyya, S.N., Buzás, E.I., Buck, A.H., de Candia, P., Chow, F.W.N., Das, S.*, et al.* (2017). Obstacles and opportunities in the functional analysis of extracellular vesicle RNA - an ISEV position paper. J Extracell Vesicles *6*, 1286095.

Matsuda, S., Rouault, J., Magaud, J., and Berthet, C. (2001). In search of a function for the TIS21/PC3/BTG1/TOB family. FEBS Lett *497*, 67-72.

McCabe, J.B., and Berthiaume, L.G. (1999). Functional Roles for Fatty Acylated Amino-terminal Domains in Subcellular Localization. Mol Biol Cell *10*, 3771-3786.

McDonald, R.A., White, K.M., Wu, J., Cooley, B.C., Robertson, K.E., Halliday, C.A., McClure, J.D., Francis, S., Lu, R., Kennedy, S.*, et al.* (2013). miRNA-21 is dysregulated in response to vein grafting in multiple models and genetic ablation in mice attenuates neointima formation. Eur Heart J *34*, 1636-1643.

McNamara, R.P., Costantini, L.M., Myers, T.A., Schouest, B., Maness, N.J., Griffith, J.D., Damania, B.A., MacLean, A.G., and Dittmer, D.P. (2018). Nef Secretion into Extracellular Vesicles or Exosomes Is Conserved across Human and Simian Immunodeficiency Viruses. MBio *9*, 559.

Morantz, R.A., Wood, G.W., Foster, M., Clark, M., and Gollahon, K. (1979a). Macrophages in experimental and human brain tumors. Part 1: Studies of the macrophage content of experimental rat brain tumors of varying immunogenicity. J Neurosurg *50*, 298-304.

Morantz, R.A., Wood, G.W., Foster, M., Clark, M., and Gollahon, K. (1979b). Macrophages in experimental and

human brain tumors. Part 2: studies of the macrophage content of human brain tumors. J Neurosurg *50*, 305-311.
Morton, M.C., Neckles, V.N., Seluzicki, C.M., Holmberg, J.C., and Feliciano, D.M. (2018). Neonatal Subventricular Zone Neural Stem Cells Release Extracellular Vesicles that Act as a Microglial Morphogen. Cell reports *23*, 78-89.
Ng, R., Song, G., Roll, G.R., Frandsen, N.M., and Willenbring, H. (2012). A microRNA-21 surge facilitates rapid cyclin D1 translation and cell cycle progression in mouse liver regeneration. The Journal of clinical investigation *122*, 1097-1108.
Nolte-'t Hoen, E.N., Buermans, H.P., Waasdorp, M., Stoorvogel, W., Wauben, M.H., and t Hoen, P.A. (2012). Deep sequencing of RNA from immune cell-derived vesicles uncovers the selective incorporation of small non-coding RNA biotypes with potential regulatory functions. Nucleic Acids Res *40*, 9272-9285.
Ostrom, Q.T., Gittleman, H., Farah, P., Ondracek, A., Chen, Y., Wolinsky, Y., Stroup, N.E., Kruchko, C., and Barnholtz-Sloan, J.S. (2013). CBTRUS statistical report: Primary brain and central nervous system tumors diagnosed in the United States in 2006-2010. Neuro-oncology *15 Suppl 2*, ii1-56.
Ostrom, Q.T., Gittleman, H., Truitt, G., Boscia, A., Kruchko, C., and Barnholtz-Sloan, J.S. (2018). CBTRUS Statistical Report: Primary Brain and Other Central Nervous System Tumors Diagnosed in the United States in 2011-2015. Neuro-oncology *20*, iv1-iv86.
Pepe, G., De Maglie, M., Minoli, L., Villa, A., Maggi, A., and Vegeto, E. (2017). Selective proliferative response of microglia to alternative polarization signals. J Neuroinflammation *14*, 236.
Põlajeva, J., Swartling, F.J., Jiang, Y., Singh, U., Pietras, K., Uhrbom, L., Westermark, B., and Roswall, P. (2012). miRNA-21 is developmentally regulated in mouse brain and is co-expressed with SOX2 in glioma. BMC Cancer *12*, 378.
Quail, D.F., and Joyce, J.A. (2017). The Microenvironmental Landscape of Brain Tumors. Cancer cell *31*, 326-341.
Roy, S., Khanna, S., Hussain, S.-R.A., Biswas, S., Azad, A., Rink, C., Gnyawali, S., Shilo, S., Nuovo, G.J., and Sen, C.K. (2009). MicroRNA expression in response to murine myocardial infarction: miR-21 regulates fibroblast metalloprotease-2 via phosphatase and tensin homologue. Cardiovasc Res *82*, 21-29.
Ruan, Q., Wang, P., Wang, T., Qi, J., Wei, M., Wang, S., Fan, T., Johnson, D., Wan, X., Shi, W*., et al.* (2014). MicroRNA-21 regulates T-cell apoptosis by directly targeting the tumor suppressor gene Tipe2. Cell Death Dis *5*, e1095-e1095.
Sawant, D.V., Wu, H., Kaplan, M.H., and Dent, A.L. (2013). The Bcl6 target gene microRNA-21 promotes Th2 differentiation by a T cell intrinsic pathway. Mol Immunol *54*, 435-442.
Sayed, D., He, M., Hong, C., Gao, S., Rane, S., Yang, Z., and Abdellatif, M. (2010). MicroRNA-21 is a downstream effector of AKT that mediates its antiapoptotic effects via suppression of Fas ligand. J Biol Chem *285*, 20281-20290.
Sayed, D., Rane, S., Lypowy, J., He, M., Chen, I.-Y., Vashistha, H., Yan, L., Malhotra, A., Vatner, D., and Abdellatif, M. (2008). MicroRNA-21 targets Sprouty2 and promotes cellular outgrowths. Mol Biol Cell *19*, 3272-3282.
Sena-Esteves, M., Tebbets, J.C., Steffens, S., Crombleholme, T., and Flake, A.W. (2004). Optimized large-scale production of high titer lentivirus vector pseudotypes. Journal of Virological Methods *122*, 131-139.
Shi, C., Liang, Y., Yang, J., Xia, Y., Chen, H., Han, H., Yang, Y., Wu, W., Gao, R., and Qin, H. (2013). MicroRNA-21 knockout improve the survival rate in DSS induced fatal colitis through protecting against inflammation and tissue injury. PloS one *8*, e66814.
Shi, R., Wang, P.-Y., Li, X.-Y., Chen, J.-X., Li, Y., Zhang, X.-Z., Zhang, C.-G., Jiang, T., Li, W.-B., Ding, W*., et al.* (2015). Exosomal levels of miRNA-21 from cerebrospinal fluids associated with poor prognosis and tumor recurrence of glioma patients. Oncotarget *6*, 26971-26981.
Singh, S.K., Marisetty, A., Sathyan, P., Kagalwala, M., Zhao, Z., and Majumder, S. (2015). REST-miR-21-SOX2 axis maintains pluripotency in E14Tg2a.4 embryonic stem cells. Stem Cell Res *15*, 305-311.
Skog, J., Würdinger, T., van Rijn, S., Meijer, D.H., Gainche, L., Sena-Esteves, M., Curry, W.T., Carter, B.S., Krichevsky, A.M., and Breakefield, X.O. (2008). Glioblastoma microvesicles transport RNA and proteins that promote tumour growth and provide diagnostic biomarkers. Nat Cell Biol *10*, 1470-1476.
Soares, R.J., Cagnin, S., Chemello, F., Silvestrin, M., Musaro, A., De Pitta, C., Lanfranchi, G., and Sandri, M.

(2014). Involvement of microRNAs in the regulation of muscle wasting during catabolic conditions. J Biol Chem *289*, 21909-21925.

Song, G., Sharma, A.D., Roll, G.R., Ng, R., Lee, A.Y., Blelloch, R.H., Frandsen, N.M., and Willenbring, H. (2010). MicroRNAs control hepatocyte proliferation during liver regeneration. Hepatology *51*, 1735-1743.

Stupp, R., Hegi, M.E., Mason, W.P., van den Bent, M.J., Taphoorn, M.J.B., Janzer, R.C., Ludwin, S.K., Allgeier, A., Fisher, B., Belanger, K.*, et al.* (2009). Effects of radiotherapy with concomitant and adjuvant temozolomide versus radiotherapy alone on survival in glioblastoma in a randomised phase III study: 5-year analysis of the EORTC-NCIC trial. Lancet Oncol *10*, 459-466.

Sugatani, T., Vacher, J., and Hruska, K.A. (2011). A microRNA expression signature of osteoclastogenesis. Blood *117*, 3648-3657.

Tamashiro, T.T., Dalgard, C.L., and Byrnes, K.R. (2012). Primary microglia isolation from mixed glial cell cultures of neonatal rat brain tissue. J Vis Exp, e3814.

Teplyuk, N.M., Mollenhauer, B., Gabriely, G., Giese, A., Kim, E., Smolsky, M., Kim, R.Y., Saria, M.G., Pastorino, S., Kesari, S.*, et al.* (2012). MicroRNAs in cerebrospinal fluid identify glioblastoma and metastatic brain cancers and reflect disease activity. Neuro-oncology *14*, 689-700.

Théry, C., Witwer, K.W., Aikawa, E., Alcaraz, M.J., Anderson, J.D., Andriantsitohaina, R., Antoniou, A., Arab, T., Archer, F., Atkin-Smith, G.K.*, et al.* (2018). Minimal information for studies of extracellular vesicles 2018 (MISEV2018): a position statement of the International Society for Extracellular Vesicles and update of the MISEV2014 guidelines. J Extracell Vesicles *7*, 1535750.

Thum, T., Gross, C., Fiedler, J., Fischer, T., Kissler, S., Bussen, M., Galuppo, P., Just, S., Rottbauer, W., Frantz, S.*, et al.* (2008). MicroRNA-21 contributes to myocardial disease by stimulating MAP kinase signalling in fibroblasts. Nature *456*, 980-984.

Tkach, M., and Théry, C. (2016). Communication by Extracellular Vesicles: Where We Are and Where We Need to Go. Cell *164*, 1226-1232.

Valadi, H., Ekström, K., Bossios, A., Sjöstrand, M., Lee, J.J., and Lötvall, J.O. (2007). Exosome-mediated transfer of mRNAs and microRNAs is a novel mechanism of genetic exchange between cells. Nat Cell Biol *9*, 654-659.

van der Vos, K.E., Abels, E.R., Zhang, X., Lai, C., Carrizosa, E., Oakley, D., Prabhakar, S., Mardini, O., Crommentuijn, M.H.W., Skog, J.*, et al.* (2016). Directly visualized glioblastoma-derived extracellular vesicles transfer RNA to microglia/macrophages in the brain. Neuro-oncology *18*, 58-69.

Vickers, K.C., Palmisano, B.T., Shoucri, B.M., Shamburek, R.D., and Remaley, A.T. (2011). MicroRNAs are transported in plasma and delivered to recipient cells by high-density lipoproteins. Nat Cell Biol *13*, 423-433.

Wang, J., Gao, Y., Ma, M., Li, M., Zou, D., Yang, J., Zhu, Z., and Zhao, X. (2013). Effect of miR-21 on renal fibrosis by regulating MMP-9 and TIMP1 in kk-ay diabetic nephropathy mice. Cell Biochem Biophys *67*, 537-546.

Wang, P., Zhao, Y., Fan, R., Chen, T., and Dong, C. (2016). MicroRNA-21a-5p Functions on the Regulation of Melanogenesis by Targeting Sox5 in Mouse Skin Melanocytes. Int J Mol Sci *17*, 959.

Wang, Z., Brandt, S., Medeiros, A., Wang, S., Wu, H., Dent, A., and Serezani, C.H. (2015). MicroRNA 21 is a homeostatic regulator of macrophage polarization and prevents prostaglandin E2-mediated M2 generation. PloS one *10*, e0115855.

Wei, F., Yang, S., Guo, Q., Zhang, X., Ren, D., Lv, T., and Xu, X. (2017a). MicroRNA-21 regulates Osteogenic Differentiation of Periodontal Ligament Stem Cells by targeting Smad5. Sci Rep *7*, 16608.

Wei, Z., Batagov, A.O., Schinelli, S., Wang, J., Wang, Y., El Fatimy, R., Rabinovsky, R., Balaj, L., Chen, C.C., Hochberg, F.*, et al.* (2017b). Coding and noncoding landscape of extracellular RNA released by human glioma stem cells. Nature Communications *8*, 1145.

Weller, M., Wick, W., Aldape, K., Brada, M., Berger, M., Pfister, S.M., Nishikawa, R., Rosenthal, M., Wen, P.Y., Stupp, R.*, et al.* (2015). Glioma. Nat Rev Dis Primers *1*, 15017.

Welm, B.E., Dijkgraaf, G.J.P., Bledau, A.S., Welm, A.L., and Werb, Z. (2008). Lentiviral transduction of mammary stem cells for analysis of gene function during development and cancer. Cell Stem Cell *2*, 90-102.

Winter, J., Jung, S., Keller, S., Gregory, R.I., and Diederichs, S. (2009). Many roads to maturity: microRNA biogenesis pathways and their regulation. Nat Cell Biol *11*, 228-234.

Wu, Z., Lu, H., Sheng, J., and Li, L. (2012). Inductive microRNA-21 impairs anti-mycobacterial responses by targeting IL-12 and Bcl-2. FEBS Lett *586*, 2459-2467.

Xie, X., Song, J., and Li, G. (2016). MiR-21a-5p suppresses bisphenol A-induced pre-adipocyte differentiation by targeting map2k3 through MKK3/p38/MAPK. Biochem Biophys Res Commun *473*, 140-146.

Yang, C.H., Yue, J., Pfeffer, S.R., Fan, M., Paulus, E., Hosni-Ahmed, A., Sims, M., Qayyum, S., Davidoff, A.M., Handorf, C.R.*, et al.* (2014). MicroRNA-21 promotes glioblastoma tumorigenesis by down-regulating insulin-like growth factor-binding protein-3 (IGFBP3). J Biol Chem *289*, 25079-25087.

Yang, C.H., Yue, J., Pfeffer, S.R., Handorf, C.R., and Pfeffer, L.M. (2011). MicroRNA miR-21 regulates the metastatic behavior of B16 melanoma cells. J Biol Chem *286*, 39172-39178.

Yang, L., Wang, B., Zhou, Q., Wang, Y., Liu, X., Liu, Z., and Zhan, Z. (2018). MicroRNA-21 prevents excessive inflammation and cardiac dysfunction after myocardial infarction through targeting KBTBD7. Cell Death Dis *9*, 769.

Ye, X., Zhang, H.M., Qiu, Y., Hanson, P.J., Hemida, M.G., Wei, W., Hoodless, P.A., Chu, F., and Yang, D. (2014). Coxsackievirus-induced miR-21 disrupts cardiomyocyte interactions via the downregulation of intercalated disk components. PLoS Pathog *10*, e1004070.

## Supplementary information

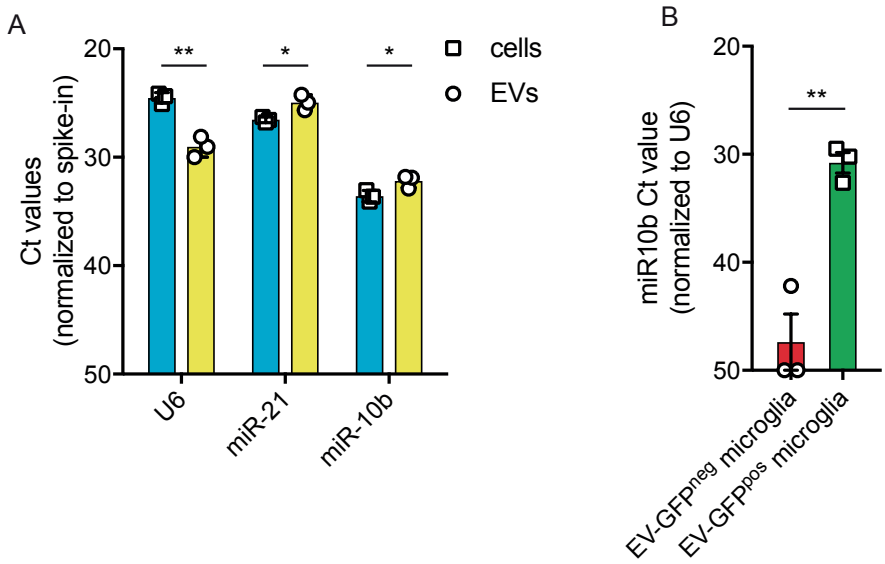


**Supplementary Figure S1**. **Glioma-specific miR-10b is present in tumor-derived EVs and is transferred to microglia**. Related to Figure 1 and 2 (**A**) Size distribution of isolated EVs analyzed using NTA showing heterogeneity of the vesicles present in the EV preparation. (**B**) miR-10b expression in cells and 2000xg fraction, as plotted in Ct normalized to spike-in (UniSp6). (**C**) miR-10b is present in cells and EV at significant different levels. (**D**) Uptake of EV-GFP results in significant elevated levels of miR-10b in microglia, with Ct>40 considered baseline. Data represents 3 independent experiments and are presented as the mean with SEM (error bars). *P<0.05, **P<0.01. Unpaired T-test.

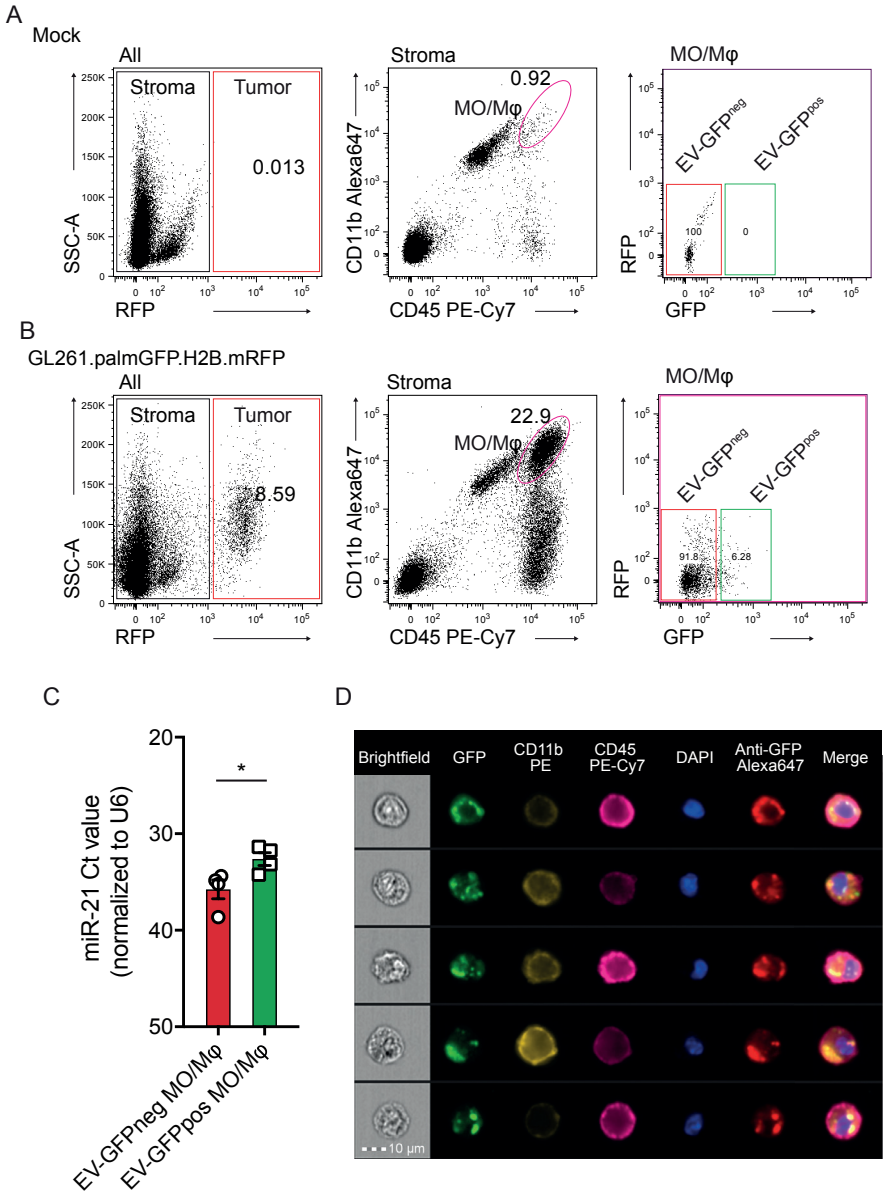


**Supplementary Figure S2. Iodixanol gradient shows co-localization of miR-21 with GFP and high-density particles**. Related to Figure 1 (**A**) Schematic overview of iodixanol gradient isolation to separate different vesicles and proteins based on density. (**B**) Presence of GFP was analyzed on different density fractions. (**C**) Fold expression of miR-21 in different fraction compared to the first fraction shows co-localization of GFP with miR-21 and miR-21 present in high-density fractions. Data represents 2 independent experiments and are presented as the mean with SEM (error bars).

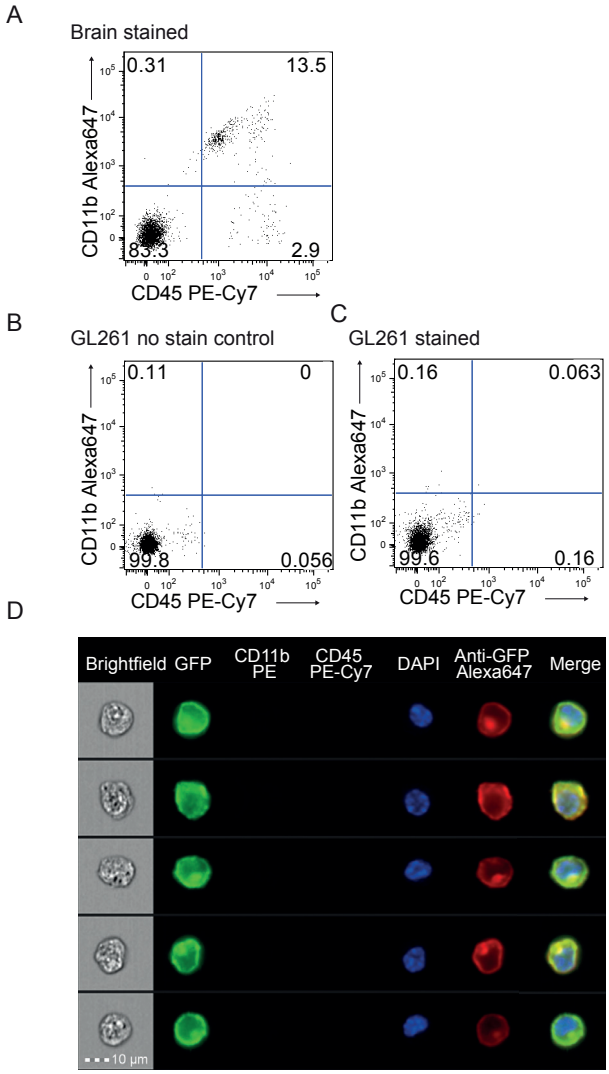


**Supplementary Figure S3. Tumor-derived EVs are taken up by CD11b$^{low}$ CD45$^{high}$ lymphocytes. Related to Figure 2 and 3** (**A**) Representative FACS plots showing gating strategy where RFP expression was used to exclude tumor cells in downstream analysis and subsequently lymphocytes were identified as CD11b$^{low}$/CD45$^{high}$ cells (yellow). Uptake of tumor derived EVs was examined based on GFP signal. (**B**) EV-GFP uptake was visualized by imaging flow cytometry using ImageStream. Scale bar 10µm.

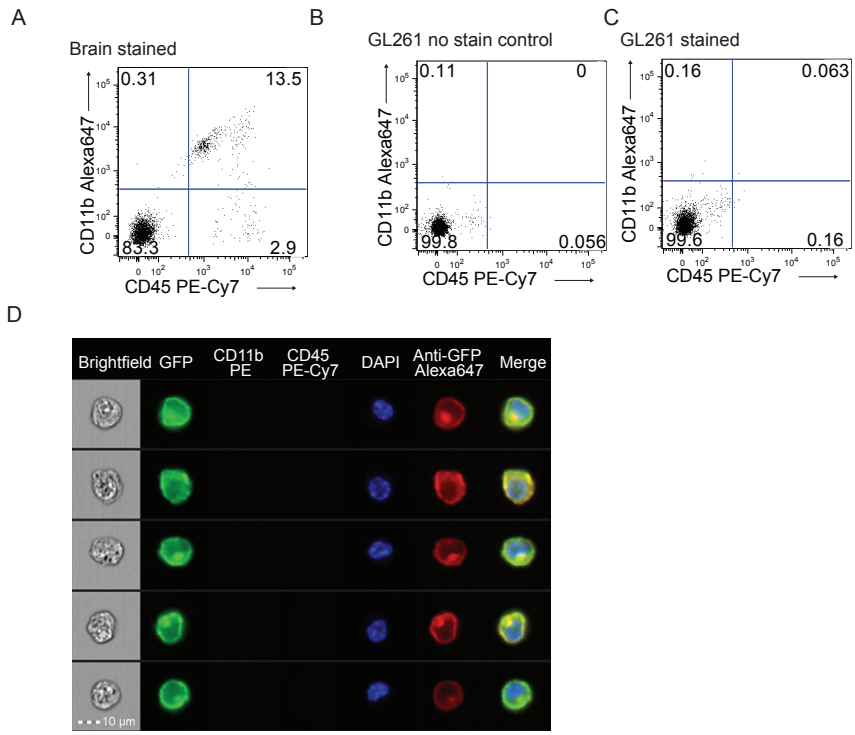


**Figure S4. GL261 cells do not express the marker used to isolate microglia, monocytes/ macrophages. Related to Figure 2 and 3** (**A**) Dissociated brain cells were stained with CD11b and CD45 to identify microglia and set limits for CD11b and CD45 expression. (**B**) The distribution of unstained GL261 cells used as negative control is shown within set gating. (**C**) GL261 cells stained with CD11b and CD45 showed that these cells do not express these markers. (**D**) Using imaging flow cytometry, GL261.palmGFP cells isolated from tumor-bearing mouse brain were imaged for anti-GFP-Alexa647. Scale bar 10 µm.

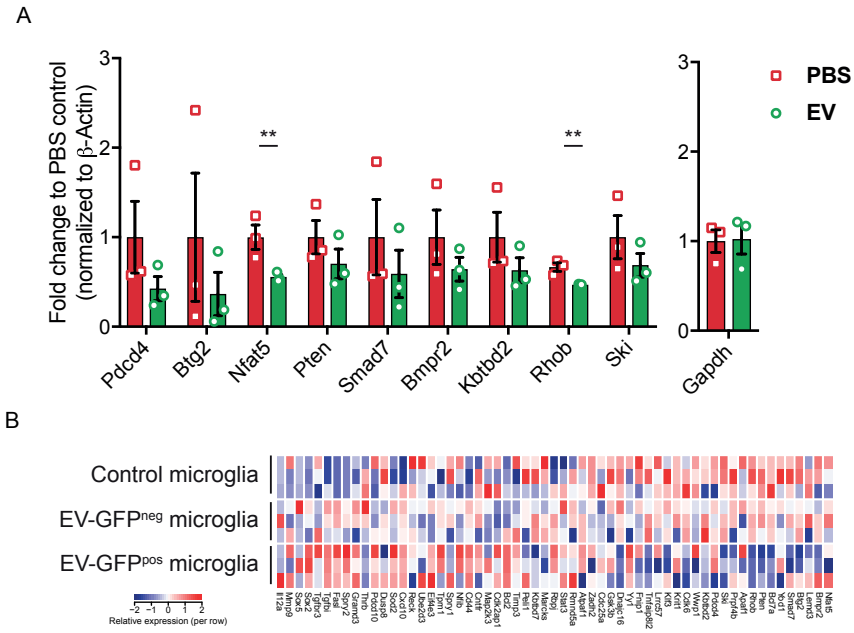


**Supplementary Figure S5. miR-21 regulates selected target genes *in vitro* and *in vivo* wild type microglia. Related to Figure 5** (**A**) EVs from conditioned media (EV) were isolated and added to wild type primary microglia followed by 24 hours incubation. Fold expression of miR-21 target genes (*Bmpr2, Btg2, Kbtbd2, Nfat5, Pdcd4, Pten, Rhob, Smad7 and Ski*) and *Gapdh*, a gene not targeted by miR-21, normalized to *β-Actin* in wild type microglia exposed to GL261-derived EVs, as compared to PBS control. Data represents 3 independent experiments and are presented as the mean with SEM (error bars). (**B**) Heatmap showing relative gene expression for 59 validated miR-21 gene targets in microglia isolated from tumor bearing mice and control isolated from miR-21 wild type mice in a similar method as displayed in Figure 2B. **P<0.01. Unpaired T-test and multiple T-test.

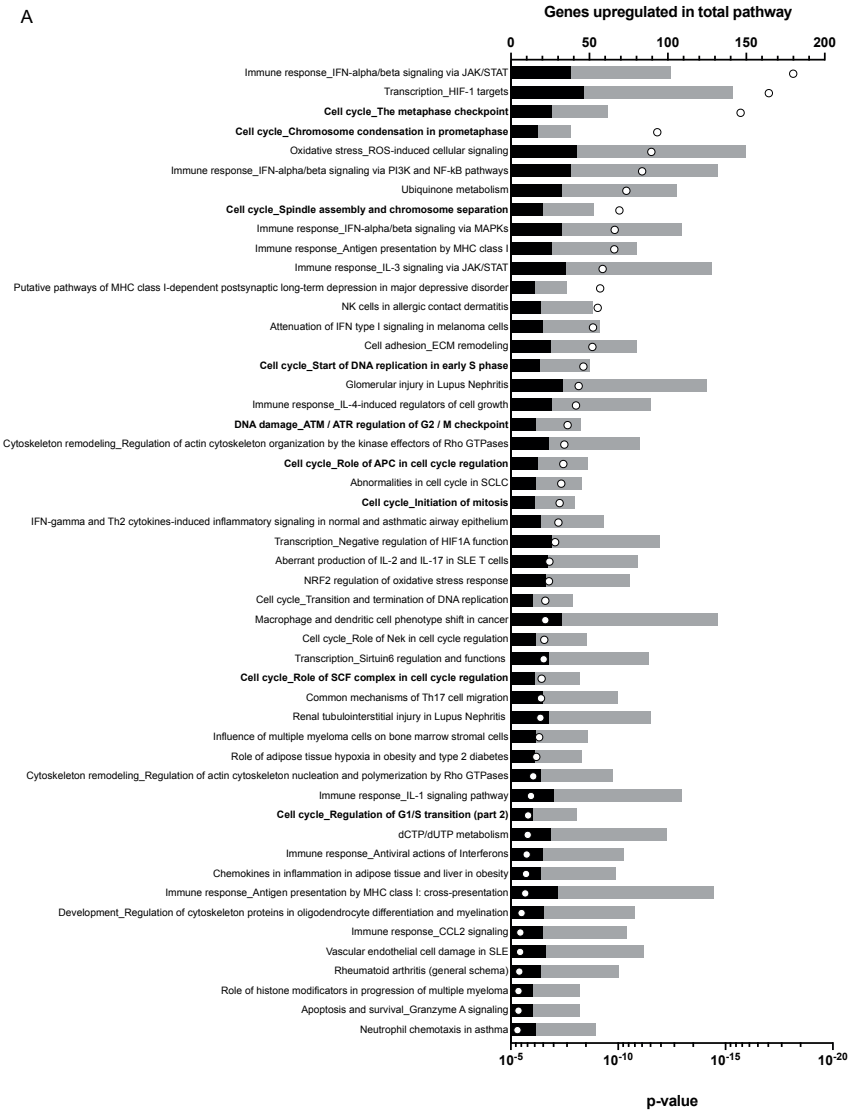


**Supplementary Figure S6. Pathway analysis of differentially expressed genes between EV-GFP$^{pos}$ and EV-GFP$^{neg}$ shows an overrepresentation of increased cell cycle control pathways.** Related to Figure 7 (**A**) Metacore pathway analysis on significantly differential expressed genes between EV-GFP$^{pos}$ and EV-GFP$^{neg}$ tumor microglia showed an overrepresentation of genes upregulated involved in cell cycle control (in bold). Genes upregulated (black) in the total pathway (grey) and p-value (circle) as associated with the pathway.

**Supplementary Table S1. miR-21 targets with method of evidence and reference. Related to Figure 4.** Mouse miR-21 target genes acquired from publically available databases (miRTarBase and miRWalk) were manually curated. Only miR-21 target genes with strong evidence (based on reporter assay, western blot and qPCR) are included.

| Gene | Evidence | | | Reference |
|---|---|---|---|---|
| | Reporter assay | Western blot | qPCR | |
| *Adgrg2* | | | ✔ | (Ma et al., 2011) |
| *Apaf1* | ✔ | | | (Hatley et al., 2010) |
| *Atpaf1* | | | ✔ | (Ma et al., 2011) |
| *Bcl2* | ✔ | | | (Wu et al., 2012) |
| *Bcl7a* | ✔ | | | (Hatley et al., 2010) |
| *Bmpr2* | | | ✔ | (McDonald et al., 2013) |
| *Btg2* | ✔ | ✔ | ✔ | (Hatley et al., 2010; Song et al., 2010; Yang et al., 2011) |
| *Cd44* | | | ✔ | (Ma et al., 2011) |
| *Cdc25a* | | ✔ | ✔ | (Kölling et al., 2017; Ma et al., 2011) |
| *Cdk2ap1* | ✔ | ✔ | ✔ | (Afonso et al., 2018) |
| *Cdk6* | | ✔ | | (Kölling et al., 2017) |
| *Cntfr* | | | ✔ | (Ma et al., 2011) |
| *Cxcl10* | | | ✔ | (Ma et al., 2011) |
| *Dnajc16* | | | ✔ | (Ma et al., 2011) |
| *Dusp8* | | | ✔ | (Ma et al., 2011) |
| *Eif4e3* | ✔ | | | (Soares et al., 2014) |
| *FasL* | ✔ | ✔ | | (Hatley et al., 2010; Sayed et al., 2010) |
| *Fnip1* | | | ✔ | (Ma et al., 2011) |
| *Gramd3* | | | ✔ | (Ma et al., 2011) |
| *Gsk3b* | ✔ | | | (Hu et al., 2017) |
| *Il12a* | ✔ | | | (Lu et al., 2009; Wu et al., 2012) |
| *Kbtbd2* | | | ✔ | (Ma et al., 2011) |
| *Kbtbd7* | ✔ | | | (Yang et al., 2018) |
| *Klf3* | | | ✔ | (Ma et al., 2011) |
| *Krit1* | | | ✔ | (Ma et al., 2011) |
| *Lemd3* | | | ✔ | (Ma et al., 2011) |
| *Lrrc57* | | | ✔ | (Ma et al., 2011) |

| | | | | |
|---|---|---|---|---|
| *Map2k3* | ✔ | | | (Hatley et al., 2010; Xie et al., 2016) |
| *Marcks* | | | ✔ | (Johnston et al., 2017) |
| *Mmp9* | | ✔ | | (Wang et al., 2013) |
| *Nfat5* | | | ✔ | (Ma et al., 2011) |
| *Nfib* | ✔ | | | (Hatley et al., 2010) |
| *Pcsk6* | | | ✔ | (Ma et al., 2011) |
| *Pdcd10* | ✔ | | | (Soares et al., 2014) |
| *Pdcd4* | ✔ | ✔ | ✔ | (Ahmed et al., 2011; Hatley et al., 2010; Lu et al., 2008; Luo et al., 2014; Sugatani et al., 2011; Yang et al., 2011) |
| *Peli1* | ✔ | | ✔ | (Marquez et al., 2010) |
| *Prpf4b* | | | ✔ | (Ma et al., 2011) |
| *Pten* | ✔ | ✔ | ✔ | (Ahmed et al., 2011; Chen et al., 2016; Lorenzen et al., 2015; Roy et al., 2009; Sayed et al., 2010; Wu et al., 2012; Yang et al., 2011) |
| *Rbpj* | | | ✔ | (Ma et al., 2011) |
| *Reck* | | | ✔ | (Hu et al., 2008) |
| *Reck* | ✔ | | | (Hatley et al., 2010) |
| *Rhob* | ✔ | | ✔ | (Hatley et al., 2010; Ng et al., 2012; Shi et al., 2013) |
| *Rmnd5a* | | | ✔ | (Ma et al., 2011) |
| *Ski* | ✔ | | | (Hatley et al., 2010) |
| *Smad7* | ✔ | ✔ | ✔ | (Hatley et al., 2010; He et al., 2016; Li et al., 2013; Lorenzen et al., 2015) |
| *Sox2* | | ✔ | | (Põlajeva et al., 2012; Singh et al., 2015) |
| *Sox5* | ✔ | ✔ | ✔ | (Wang et al., 2016) |
| *Sox7* | | | ✔ | (Ma et al., 2011) |
| *Spry1* | ✔ | | ✔ | (Sawant et al., 2013; Thum et al., 2008) |
| *Spry2* | ✔ | ✔ | | (Hatley et al., 2010; Sayed et al., 2008) |
| *Stat3* | ✔ | | | (Wang et al., 2015) |
| *Tgfbi* | ✔ | ✔ | | (Liu et al., 2011) |

| | | | | |
|---|---|---|---|---|
| *Tgfbr3* | ✔ | ✔ | ✔ | (Liang et al., 2012) |
| *Thrb* | | | ✔ | (Ma et al., 2011) |
| *Timp3* | | | ✔ | (Ahmed et al., 2011; Fiorentino et al., 2013) |
| *Tnfaip8l2* | | | ✔ | (Ruan et al., 2014) |
| *Tpm1* | | | ✔ | (Ahmed et al., 2011) |
| *Ube2d3* | | | ✔ | (Ma et al., 2011) |
| *Wwp1* | | | ✔ | (Ma et al., 2011) |
| *Yod1* | ✔ | | ✔ | (Ma et al., 2011; Ye et al., 2014) |
| *Yy1* | ✔ | | | (Soares et al., 2014) |
| *Zadh2* | | | ✔ | (Ma et al., 2011) |